47-Electron Organometallic Clusters Derived by Chemical and Electrochemical Oxidation of Trihydrido(alkylidyne)triruthenium and -triosmium Clusters. Ligand Additivity in Metal Clusters

William G. Feighery,† Huirong Yao, Anthony F. Hollenkamp,‡ Robert D. Allendoerfer, and Jerome B. Keister*

Department of Chemistry, University at Buffalo, State University of New York, Buffalo, New York 14260-3000

Received August 29, 1997

Cyclic voltammograms for $H_3Ru_3(\mu_3\text{-}CX)(CO)_{9-n}L_n$ (X = OMe, SEt, Me, Et, Ph, NMeBz, Br; L = PR_3, $AsPh_3$, $SbPh_3$; $n = 2, 3$), $H_3Ru_3(\mu_3\text{-}COMe)(CO)_6(PPh_3)_2(L)$ (L = $P(OMe)_3$, $CNCH_2Ph$), and $H_3Os_3(\mu_3\text{-}COMe)(CO)_7(PPh_3)_2$ each display a quasi-reversible to reversible, one-electron oxidation followed by an irreversible to quasi-reversible, one-electron oxidation. The ligand and substituent effects upon the oxidation potential are analyzed as an example of ligand additivity in a cluster system; the oxidation potential of the alkylidyne cluster core is as sensitive to π-donor substituent effects as are aromatic π complexes such as $CpFe(C_5H_4X)$ to substituents on the rings, and the dependence of the oxidation potential of the cluster upon ligand substitution on any given Ru atom is 37% of that expected for the oxidation of a monometallic complex. Reactions with 1 equiv of Ag^+ or ferricenium give the 47-electron cations $[H_3Ru_3(CX)(CO)_6L_3]^{1+}$ (X = OMe; $L_3 = (PPh_3)_2L'$; L′ = CO, PPh_3, $P(OMe)_3$, $CNCH_2Ph$; X = Ph, NMeBz, SEt, L = PPh_3), characterized by EPR spectroscopy; the equilibrium between isomers $H_3Ru_3(COMe)(CO)_6(ax\text{-}PPh_3)_2$(ax- and eq-$PPh_3)^{0/1+}$ (ax = axial coordination, eq = equatorial coordination) favors the axial coordination for the 48-electron cluster (eq/ax = 0.15) and equatorial coordination for the 47-electron species (eq/ax = 6.4). The rate constant for ax−eq isomerization for the 47-electron species (6.5 s^{-1}) is 4 orders of magnitude greater than that for the 48-electron species (2×10^{-4} s^{-1}). The 47-electron clusters have lifetimes which are correlated with the oxidation potentials of the precursors, ranging from seconds to many hours at room temperature. Slow decomposition of $[H_3Ru_3(COMe)(CO)_6L_3]^{1+}$ in the absence of added CO forms the new 46-electron clusters $[H_3Ru_3(CO)_7L_3]^{1+}$ (L = PPh_3, $AsPh_3$). $[H_3Ru_3(COMe)(CO)_6(PPh_3)_3]^{1+}$ does not react with CCl_4 but does react with Lewis bases such as CO and acetonitrile. Disproportionation occurs with acetonitrile, chloride, and pyridine; the CO products are $[HRu_3(CO)_9(PPh_3)_3]^{1+}$, $[MePPh_3]^{1+}$, and $H_3Ru_3(COMe)(CO)_{9-n}(PPh_3)_n$ ($n = 1, 2$).

Introduction

The redox properties of molecular metal clusters are of interest with respect to the chemical reactivity of radicals,[1] novel electrical properties of organometallics,[2] and fundamental chemistry of metal−metal bonds.[3] Electrochemical studies of organometallic clusters have received increasing attention because of the importance of odd-electron intermediates in many reaction mechanisms and also because of examples of structural changes of the metal cluster framework induced by electrochemical oxidations or reductions.[3] Radical cations formed by oxidation of saturated dinuclear complexes are usually very unstable with respect to fragmentation. Odd-electron clusters of three or more metal atoms, especially clusters capped by main-group atoms, seem to be more stable than dinuclear odd-electron species.

The electrochemistry of alkylidynetrimetallic clusters has been the subject of a number of studies.[4] The most extensive studies have concerned $Co_3(CX)(CO)_9$ and substituted derivatives. The HOMO for this series has Co−Co bonding character.[5] These clusters undergo one-electron reductions to form 49-electron radical anions, and phosphine-substituted derivatives can be oxidized;

† Present address: Chemistry Department, Indiana University at South Bend, South Bend, IN 46615.

‡ On leave from the Commonwealth Scientific and Industrial Research Organization (CSIRO), Division of Minerals, Port Melbourne, Victoria, 3207, Australia.

(1) (a) Brown, T. L. In *Organometallic Radical Processes*; Trogler, W. C., Ed.; Elsevier: Amsterdam, 1990; p 67. (b) Kochi, J. K. *J. Organomet. Chem.* **1986**, *300*, 139. (c) Tyler, D. R. *Prog. Inorg. Chem.* **1988**, *36*, 125. (e) Connelly, N. G. *Chem. Soc. Rev.* **1989**, *18*, 153. (f) Geiger, W. E. *Prog. Inorg. Chem.* **1985**, *33*, 275. (g) Trogler, W. C. In *Organometallic Radical Processes*; Trogler, W. C., Ed.; Elsevier: Amsterdam, 1990; p 306.

(2) Astruc, D. *Electron Transfer and Radical Processes in Transition-Metal Chemistry*; VCH Publishers, Inc.: New York, 1995; Chapter 4.

(3) (a) Lemoine, P. *Coord. Chem. Rev.* **1982**, *47*, 55. (b) Lemoine, P. *Coord. Chem. Rev.* **1988**, *83*, 169. Other leading references: (c) Etienne, M.; Mathieu, R.; Lugan, N. *Organometallics* **1993**, *12*, 140. (d) Pugh, J. R.; Meyer, T. J. *J. Am. Chem. Soc.* **1992**, *114*, 3784. (e) Bullock, J. P.; Palazotto, M. C.; Mann, K. R. *Inorg. Chem.* **1991**, *30*, 1284. (f) Connelly, N. G.; Geiger, W. E. *Adv. Organomet. Chem.* **1985**, *24*, 87.

S0276-7333(97)00769-3 CCC: $15.00
Publication on Web 02/11/1998

however, the products are not very stable. The redox series $[FcCCo_3(CO)_6\ L_3]^{2+/1+/0/1-}$ (Fc = ferrocenyl) was examined by electrochemical methods.[4i,j] The first oxidation corresponds to the ferrocenyl moiety, whereas the second involves the Co_3C unit. The [1+,1+] species could be prepared by chemical oxidation. A linear relationship between $E_{1/2}$[1,0] and the number of PR_3 ligands was noted. Mixed-metal analogues have also been studied.[4f,g,h]

The 49/48/47-electron species $[Co_3(\mu_3\text{-CPh})_2Cp_3]^{1-/0/1+}$ have been generated electrochemically. The 48/47-electron oxidation is at 0.34 V vs SCE and is electrochemically reversible. The 47-electron cation displays a broad EPR signal at $g = 2.2$. The HOMO of the 48-electron cluster is a degenerate pair, implying a Jahn−Teller distorted 47-electron species.[6]

The electrochemistry of $Ru_3(\mu_3\text{-CMe})(\mu\text{-CO})_3(\eta^5\text{-}C_5Me_5)_3$ displays two electrochemically reversible one-electron oxidations at 0.17 and 0.86 V (reference not specified).[7] The strong donor Cp* ligands stabilize the 47-electron product, so much so that the radical cation could be isolated and crystallographically characterized. The structure has approximate C_{3v} symmetry. While no EPR signal was detectable, a magnetic moment of 2.0 μ_B was measured. The 46-electron species was also isolated; deprotonation generated the vinylidene $[Ru_3(\mu_3\text{-}\eta^2\text{-CCH}_2)(\mu\text{-CO})_3(\eta^5\text{-}C_5Me_5)_3]^{1+}$.

The class of clusters $H_3Ru_3(\mu_3\text{-CX})(CO)_{9-n}(PPh_3)_n$ is closely related to the tricobalt series, but the presence of hydride ligands and differences in the nature of the HOMO as a result make the reaction chemistry very different.[8] The HOMO is Ru−CX bonding in nature and involves π conjugation with a filled p orbital of the X substituent, so that a one-electron oxidation should generate a radical cation in which the SOMO has metal−carbon bonding character.[9] We report here, concerning the electrochemical properties of these compounds, the characterization of 47-electron radical cation oxidation products and also some chemical reactions of these 47-electron clusters. A preliminary account of some of this work has appeared previously.[10]

Experimental Section

Starting Materials. $HRu_3(\mu\text{-CNMeBz})(CO)_{10}$,[11] $H_3Ru_3(COMe)(CO)_9$,[12] $H_3Os_3(COMe)(CO)_9$,[12] $H_3Ru_3(CPh)(CO)_9$,[13] $H_3Ru_3(CSEt)(CO)_9$,[14] $H_3Ru_3(CX)(CO)_{9-n}L_n$ (X = MeO, Me, Ph; n = 2, 3; L = $AsPh_3$),[15] $HRu_3(COMe)(CO)_{10-n}L_n$,[16] $H_2Os_3(CO)_{10}$,[17] $H_2Os_3(CO)_9(PPh_3)$,[18] and $H_3Ru_3(CNMeBz)(CO)_6(SbPh_3)_3$[11] were prepared as previously described. Synthetic procedures for the preparation of $H_3Ru_3(COMe)(CO)_6(PPh_3)_3$[15] and $H_3Ru_3(CPh)(CO)_6(PPh_3)_3$[15] have been previously published; however, these procedures have been modified, and the new preparations are described in the Supporting Information. Dichloromethane was distilled under nitrogen from calcium hydride before use. Other chemicals were of reagent grade purity and were used as received. All manipulations were carried out under a blanket of nitrogen and with nitrogen-saturated solvents using standard Schlenk procedures. However, workup and spectral analyses were conducted without exclusion of air.

Physical Methods of Characterizations. Infrared spectra were recorded on Mattson Instruments Alpha Centauri FTIR, Nicolet Magna 550 FTIR, or Beckman 4250 spectrophotometers. ^{1}H NMR spectra were obtained on JEOL FX-90, Varian Associates Gemini 300, or Varian Associates VXR-400S instruments, using deuteriochloroform or dichloromethane-d_2 as the solvent and TMS as the reference. ^{13}C NMR spectra were recorded either on the Gemini 300 or the VXR-400S instrument in deuteriochloroform and referenced to TMS. ^{31}P NMR spectra were recorded on the VXR-400S instrument in deuteriochloroform, and chemical shifts are reported relative to o-phosphoric acid. EPR spectra were recorded on an IBM/Bruker X-band ER-200 SRC spectrometer, with a microwave power of 20 mW, in dichloromethane solution.[20]

$H_3Ru_3(CNMeBz)(CO)_6(PPh_3)_3$. To a solution of $HRu_3(CNMeBz)(CO)_{10}$ (105 mg) in 50 mL of cyclohexane was added 150 mg (4 equiv) of PPh_3. Hydrogen gas was bubbled through the solution, and it was heated at reflux for 8 h, during which time the color changes from yellow to red. The solvent was removed, and the product recrystallized from a dichloromethane/methanol mixture. Yield: 157 mg, 77%. Anal. Calcd for $Ru_3C_{69}H_{58}O_6P_3N$: C, 59.48; H, 4.19. Found: C, 59.11; H, 3.98.

$H_3Ru_3(CSEt)(CO)_6(PPh_3)_3$. To a solution of $H_3Ru_3(CSEt)(CO)_9$ (105.1 mg) in 15 mL of dichloromethane was added 176.6 mg (4 equiv) of PPh_3. This solution was stirred under nitrogen at room temperature overnight. The solvent was removed, and the product was recrystallized from a dichloromethane/methanol mixture. Yield: 203.6 mg, 92%. Anal. Calcd for $Ru_3C_{63}H_{53}O_6P_3S$: C, 56.71; H, 4.00. Found: C, 57.02; H, 3.99.

$H_3Ru_3(COMe)(CO)_6(PPh_3)_2(CNCH_2Ph)$. The reaction of $H_3Ru_3(COMe)(CO)_7(PPh_3)_2$ (2.3 mM) and CNBz (2.4 mM) in $CDCl_3$ (0.7 mL) was monitored by ^{1}H NMR spectroscopy. The substitution initially produced $H_3Ru_3(COMe)(CO)_6(PPh_3)_2$(ax-CNBz), which isomerized to an equilibrium mixture (eq/ax = 88/12) with $H_3Ru_3(COMe)(CO)_6(PPh_3)_2$(eq-CNBz). TLC of the residue on silica eluting with 2:1 dichloromethane:hexanes yielded 18 mg, 51%. Anal. Calcd for $Ru_3C_{52}H_{43}NO_7P_3$: C, 53.89; H, 3.74. Found: C, 53.72; H, 3.71.

Rate constants were determined from the integrals of the hydride resonances. The rate constant for the initial substitution was determined from the slope of a plot of ln(mol fraction of $H_3Ru_3(COMe)(CO)_7(PPh_3)_2$) vs time ($k_{sub} = 9.8 \times 10^{-5}$ sec^{-1}

(4) (a) Peake, B. M.; Robinson, B. H.; Simpson, J.; Watson D. J. *Inorg. Chem.* **1977**, *16*, 405. (b) Bond, A. M.; Peake, B. M.; Robinson, B. H.; Simpson, J.; Watson, D. J. *Inorg. Chem.* **1977**, *16*, 410. (c) Bond, A. M.; Dawson, P. A.; Peake, B. M.; Reiger, P. H.; Robinson, B. H.; Simpson, J. *Inorg. Chem.* **1979**, *18*, 1413. (d) Downard, A. J.; Robinson, B. H.; Simpson, J. *Organometallics* **1986**, *5*, 1122. (e) Kotz, J. C.; Petersen, J. V.; Reed, R. C. *J. Organomet. Chem.* **1976**, *120*, 433. (f) Lindsay, P. N.; Peake, B. M.; Robinson, B. H.; Simpson, J.; Honrath, U.; Vahrenkamp, H.; Bond, A. M. *Organometallics* **1984**, *3*, 413. (g) Honrath, U.; Vahrenkamp, H. *Z. Naturforsch.* **1984**, *39b*, 545. (h) Honrath, U.; Vahrenkamp, H. *Z. Naturforsch.* **1984**, *39b*, 555. (i) Colbran, S. B.; Robinson, B. H.; Simpson, J. *Organometallics* **1983**, *2*, 952. (j) Colbran, S. B.; Robinson, B. H.; Simpson, J. *Organometallics* **1983**, *2*, 943. (k) Downard, A. J.; Robinson, B. H.; Simpson, J. *Organometallics* **1986**, *5*, 1132. (l) Downard, A. J.; Robinson, B. H.; Simpson, J. *Organometallics* **1986** *5*, 1140. (m) Robinson, B. H.; Simpson, J.; Trounson, M. E. *Aust. J. Chem.* **1986**, *39*, 1435. (n) Worth, G. H.; Robinson, B. H.; Simpson, J. *Organometallics* **1992**, *11*, 3863.

(5) Chesky, P. T.; Hall, M. B. *Inorg. Chem.* **1981**, *20*, 4419.

(6) Enoki, S.; Kawamura, T.; Yonezawa, T. *Inorg. Chem.* **1983**, *22*, 3821.

(7) Connelly, N. G.; Forrow, N. J.; Knox, S. A. R.; Macpherson, K. A.; Orpen, A. G. *J. Chem. Soc., Chem. Commun.* **1985**, 16.

(8) Keister, J. B. *Polyhedron* **1988**, *7*, 847.

(9) Sherwood, D. E., Jr.; Hall, M. B. *Organometallics* **1982**, *1*, 1519.

(10) (a) Feighery, W. G.; Allendoerfer, R. D.; Keister, J. B. *Organometallics* **1990**, *9*, 2424. (b) Churchill, M. R.; Lake, C. H.; Feighery, W. G.; Keister, J. B. *Ibid.* **1991**, *10*, 2384.

(11) Keister, J. B.; Payne, M. W.; Muscatella, M. J. *Organometallics* **1983**, *2*, 219.

(12) Keister, J. B.; Shapley, J. R.; Strickland, D. A. *Inorg. Synth.* **1990**, *27*, 196.

(13) Keister, J. B.; Horling, T. L. *Inorg. Chem.* **1980**, *19*, 2304.

(14) Churchill, M. R.; Ziller, J. W.; Dalton, D. M.; Keister, J. B. *Organometallics* **1987**, *6*, 806.

(15) Rahman, Z. A.; Beanan, L. R.; Bavaro, L. M.; Modi, S. P.; Keister, J. B.; Churchill, M. R. *J. Organomet. Chem.* **1984**, *263*, 75.

(16) Dalton, D. M.; Barnett, D. J.; Duggan, T. P.; Keister, J. B.; Malik, P. T.; Modi, S. P.; Shaffer, M. R.; Smesko, S. A. *Organometallics* **1985**, *4*, 1854

(17) Kaesz, H. D. *Inorg. Synth.* **1990**, *28*, 238.

(18) Deeming, A. J.; Hasso, S. *J. Organomet. Chem.* **1976**, *114*, 313.

at 19 °C). Rate constants for isomerization were determined from a nonlinear least-squares fit of the equation $[ax] - [ax]_{eq} = (k_a[S]_0/(k_b - 9.8 \times 10^{-5}\ s^{-1}))\exp(-9.8 \times 10^{-5}\ s^{-1}\ t) + ([ax]_0 - ((k_a[S]_0)/(k_b - 9.8 \times 10^{-5}\ s^{-1}))\exp(-k_b t)$, where [ax] and $[ax]_{eq}$ are the mole fractions of the axial isomer at time t and at equilibrium, respectively, $[S]_0$ and $[ax]_0$ are the mole fractions of the starting material and the axial isomer at $t = 0$, $k_a = k_{sub} - k_r$, and $k_b = k_f + k_r$. The forward and reverse rate constants for isomerization of $H_3Ru_3(COMe)(CO)_6(PPh_3)_2$(ax-CNBz) to $H_3Ru_3(COMe)(CO)_6(PPh_3)_2$(eq-CNBz) are $k_f = 8.8 \times 10^{-5}$ and $k_r = 1.2 \times 10^{-5}\ s^{-1}$, respectively.

The product could also be obtained by reaction of CNBz with $H_3Ru_3(COMe)(CO)_6(PPh_3)_3$. Over a several hour period, the disappearance of $H_3Ru_3(COMe)(CO)_6(PPh_3)_3$ and formation of a mixture of axially and equatorially substituted $H_3Ru_3(COMe)(CO)_6(PPh_3)_2$(CNBz) was observed. The initial product mixture was richer in the axially substituted isomer, but overnight the equilibrium mixture was obtained.

$H_3Ru_3(COMe)(CO)_6(PPh_3)_2(P(OMe)_3)$. A solution of $H_3Ru_3(COMe)(CO)_7(PPh_3)_2$ (32 mg, 0.030 mmol) and $P(OMe)_3$ (3.9 μL, 0.033 mmol) in dichloromethane (30 mL) was stirred under nitrogen for 9 h. TLC on silica eluting with 2:1 dichloromethane:hexanes yielded two yellow bands characterized as $H_3Ru_3(COMe)(CO)_6(PPh_3)_2(P(OMe)_3)$ (17.5 mg, 50%) and $H_3Ru_3(COMe)(CO)_6(PPh_3)(P(OMe)_3)_2$ (9.4 mg, 30%) in order of elution. Anal. Calcd for $Ru_3C_{47}H_{45}O_{10}P_3$: C, 48.415; H, 3.89. Found: C, 48.22; H, 3.99.

$H_3Os_3(COMe)(CO)_{9-n}(PPh_3)_n$ (n = 1, 2). To a stirred solution of $H_3Os_3(COMe)(CO)_9$ (127 mg) in cyclohexane (20 mL) was added PPh_3 (39 mg, 1 equiv). The solution was heated to reflux under a nitrogen atmosphere for 24 h. The products were separated by thin-layer chromatography on silica gel, eluting with a 5:1 cyclohexane:dichloromethane mixture, affording three yellow bands. The top band was unreacted starting material (30 mg, 24%) followed by the monosubstituted product (51 mg, 32%) and then by the di-substituted product (60 mg, 31%). Anal. Calcd for $Os_3C_{45}H_{36}O_8P_2$: C, 40.42; H, 2.71. Found: C, 40.50; H, 2.53.

Chemical Oxidation of Substituted Alkylidyne Clusters. For each of the clusters $H_3Ru_3(CX)(CO)_{9-n}L_n$ (X = OMe, L = $AsPh_3$ and PPh_3, n = 0−3; X = NMeBz, L = PPh_3, n = 3, X = SEt, L = PPh_3, n = 3; X = Ph, L = PPh_3, n = 3), $H_3Ru_3(COMe)(CO)_6(PPh_3)_2L$ (L = $CNCH_2Ph$, $P(OMe)_3$), and $H_3Os_3(COMe)(CO)_{9-n}(PPh_3)_n$ (n = 0−2), the procedure for the oxidation was as follows. To a dichloromethane solution of the cluster was added 1 equiv of the oxidant ($[Fe(o\text{-}phen)_3](ClO_4)_3$, $AgCF_3SO_3$, $AgBF_4$, or $FeCp_2PF_6$) under nitrogen. The solution immediately turned from yellow/orange to green. The solvent was removed under vacuum. For ESR analysis, the mixture was dissolved in a small amount of dichloromethane (approximately 10^{-3} M in cluster), filtered into an ESR tube, and vacuum sealed. For NMR analysis, the mixture was dissolved in $CDCl_3$ and filtered into an NMR tube.

Reduction of $[H_3Ru_3(COMe)(CO)_6(PPh_3)_3]^{1+}$. To a solution of 19.6 mg of $H_3Ru_3(COMe)(CO)_6(PPh_3)_3$ in dichloromethane was added 4.8 mg (1 equiv) of $AgCF_3SO_3$. The solution turned green. A freshly prepared solution of Na/benzophenone in THF was then added dropwise until the cluster solution turned from green to orange. After the solvent was removed and redissolution in $CDCl_3$, the ^1H NMR spectrum showed that only $H_3Ru_3(COMe)(CO)_6(PPh_3)_3$ was present. After TLC, the starting material was recovered (18.1 mg, 93% yield).

Decomposition of $[H_3Ru_3(COMe)(CO)_6(PPh_3)_3]^{1+}$ to $[H_3Ru_3(CO)_7(PPh_3)_3]^{1+}$. To a solution of $H_3Ru_3(COMe)(CO)_6(PPh_3)_3$ (30 mg) in $CDCl_3$ (0.7 mL) was added 2 μL of toluene. The methyl proton resonance of toluene was used as a reference peak to measure the relative amounts of clusters present during various stages of the reaction. Oxidation of the cluster with 1 equiv of Ag^+ turned the color of the solution from orange to green. A small amount of water (ca. 5 μL) was added. After the mixture was allowed to stand overnight, the NMR spectrum contained resonances due to $[H_3Ru_3(CO)_7(PPh_3)_3]^+$ (42%) and $H_3Ru_3(COMe)(CO)_6(PPh_3)_3$ (30%), the yields determined by integration versus the toluene standard. No other hydride resonances were observed.

A solution of $[H_3Ru_3(COMe)(CO)_6(PPh_3)_3]^{1+}$, prepared by reaction of $H_3Ru_3(COMe)(CO)_6(PPh_3)_3$ (27 mg, 20 μmol) with $AgSO_3CF_3$ (5 mg, 23 μmol) in dichloromethane (20 mL), was allowed to stand overnight under nitrogen. Following evaporation of the solution to dryness, the ^1H NMR spectum of the residue in deuteriochloroform showed the presence of $[H_3Ru_3(CO)_7(PPh_3)_3]^{1+}$, a doublet at 2.54 ppm attributed to $MePPh_3^{1+}$, and very broad resonances at −15.2 and 4.2 ppm assigned to $[H_3Ru_3(COMe)(CO)_6(PPh_3)_3]^{1+/0}$. Carbon monoxide was bubbled through the solution to decompose the remaining radical cation and to convert $[H_3Ru_3(CO)_7(PPh_3)_3]^{1+}$ to the red species believed to be $[HRu_3(CO)_9(PPh_3)_3]^{1+}$. The spectrum now showed the presence of $H_3Ru_3(COMe)(CO)_6(PPh_3)_3$ (−15.1 ppm), $H_3Ru_3(COMe)(CO)_7(PPh_3)_2$ (−15.85, −16.35 ppm), $H_3Ru_3(COMe)(CO)_8(PPh_3)$ (−16.9, −17.5 ppm), $[HRu_3(CO)_9(PPh_3)_3]^{1+}$ (−17.05 ppm) and $MePPh_3^{1+}$ (2.54 ppm), in molar ratios of 0.18:0.86:0.16:1:1.

Reactions of $H_3Ru_3(COMe)(CO)_6(PPh_3)_3^{1+}$ with Carbon Monoxide. Carbon monoxide was bubbled through a solution of $[H_3Ru_3(COMe)(CO)_6(PPh_3)_3]^{1+}$, prepared by reaction of $H_3Ru_3(COMe)(CO)_6(PPh_3)_3$ (50.3 mg, 38.6 μmol) with $FeCp_2PF_6$ (14.1 mg, 42.5 μmol) in dichloromethane (20 mL). The color of the solution rapidly changed from yellow-green to red. IR spectra were taken periodically until no further change was noted after 2 h. The solution was evaporated to dryness, and the residue was applied to a silica gel TLC plate, which was eluted with dichloromethane/hexanes (1:1 v/v) to remove ferrocene (isolated 7.0 mg) and $H_3Ru_3(COMe)(CO)_{9-n}(PPh_3)_n$ (n = 3, 11.6 mg (23%); n = 2, 2.4 mg, impure). The bottom red band was extracted with ethyl acetate/dichloromethane; evaporation yielded 40.5 mg of a red solid. The red material was dissolved in a minimum amount of methanol, and a methanol solution of sodium tetraphenylborate (16.1 mg, 46.8 μmol) was added. A red-purple precipitate was collected by filtration and washed with methanol. This material is likely a mixture of products. The red solid was dissolved in dichloromethane, filtered, and then recrystallized from dichloromethane−methanol at −20 °C. Red-purple crystals were isolated from the near-colorless solution. (18.9 mg, 11.4 μmol, 29.5% based upon starting material). IR (CH_2Cl_2): 2096 vw, 2064 m, 2026 vs, 2011 sh, 1992 vw sh, 1967 vw cm^{-1}.[1] ^1H NMR ($CDCl_3$): −17.05 (dt, J_{PH} 3, 6 Hz) ppm. ^{31}P NMR ($CDCl_3$), PF_6 salt: 26.1 (1 P, d, J 12 Hz), 29.2 (1 P, s), 32.6 (1 P, d, J 12 Hz), −144.5 (1 P, sept, J_{PF} 714 Hz), 29.2 (0.2 P, s) ppm. MS (positive-ion FAB), PF_6 salt: m/e M^+ 1345, $(M - CO)^+$ 1317 ($^{102}Ru_3$). Anal. Calcd for $BRu_3C_{87}H_{66}O_9P_3$: C, 62.86; H, 4.00. Found: C, 62.09; H, 4.00.

Carbon Tetrachloride. Oxidation of $H_3Ru_3(COMe)(CO)_6(PPh_3)_3$ (0.86 mM) was achieved by addition of ferricinium hexafluorophosphate. IR analysis indicated complete conversion to $[H_3Ru_3(COMe)(CO)_6(PPh_3)_3]^{1+}$. A 5 mL portion was transferred to a second flask, and carbon tetrachloride (7 μL, 17 equiv) was added. No differences between the IR spectra of the two solutions were noted after 25 min.

Acetonitrile. To a 5 mL portion of the solution prepared as described above was added acetonitrile (7.0 μL, 30 equiv). The color of the solution immediately began to change from yellow-green to dark red. After 30 min, the IR spectrum of the solution contained absorptions at 2065 w, 2036 s, 2009 s, 1973 m, and 1960 m cm^{-1}. Chromatographic workup allowed the recovery of $H_3Ru_3(COMe)(CO)_6(PPh_3)_3$ in 27% yield.

Pyridine. The addition of pyridine (5 μL, 7.7 equiv) to a solution of $[H_3Ru_3(COMe)(CO)_6(PPh_3)_3]^+$ (formed from 10.5 mg $H_3Ru_3(COMe)(CO)_6(PPh_3)_3$ and $FeCp_2PF_6$ (2.7 mg) in 5 mL CH_2Cl_2) caused the color of the solution to change from green-yellow to red-orange within 15 min. The IR spectrum con-

tained absorptions due to $H_3Ru_3(COMe)(CO)_6(PPh_3)_3$ in addition to a broad absorption at 2060 cm^{-1}.

Chloride. The addition of PPNCl (6.2 mg, 1.2 equiv) to a solution of $[H_3Ru_3(COMe)(CO)_6(PPh_3)_3]^+$ (formed from 11.7 mg $H_3Ru_3(COMe)(CO)_6(PPh_3)_3$ and $FeCp_2PF_6$ (3.2 mg) in 6 mL CH_2Cl_2) caused the color to change from green-yellow to yellow upon mixing. The IR spectrum contained absorptions due the $H_3Ru_3(COMe)(CO)_6(PPh_3)_3$ (ca. 67% recovery).

Triphenylphosphine. Addition of PPh_3 (11.2 mg) to a solution of $[H_3Ru_3(COMe)(CO)_6(PPh_3)_3]^+$ (formed from 25.2 mg $H_3Ru_3(COMe)(CO)_6(PPh_3)_3$ and $AgSO_3CF_3$ (ca. 8 mg)) resulted in slow changes over a 40 min period. After 24 h, the solution was evaporated to dryness. The ^1H NMR spectrum ($CDCl_3$ solution) displayed signals at 3.90 (br) and −15.2 (br) ppm assigned to $[H_3Ru_3(COMe)(CO)_6(PPh_3)_3]^{0/+}$, 2.92 (d, J 13 Hz) ppm, assigned to $[MePPh_3]^{1+}$, and −11.1 (br), −11.55 (br d), and −12.3 (br) assigned to $[H_3Ru_3(CO)_7(PPh_3)_3]^+$. A ratio of $MePPh_3]^{1+}/[H_3Ru_3(CO)_7(PPh_3)_3]^{1+}$ of 1.1 was determined. Next, carbon monoxide was bubbled through solution for a few minutes, causing an immediate color change to red. The NMR spectrum displayed hydride resonances due to $H_3Ru_3(COMe)(CO)_6(PPh_3)_3$, $H_3Ru_3(COMe)(CO)_7(PPh_3)_2$, and $[HRu_3(CO)_9(PPh_3)_3]^{1+}$ in molar ratios of 1.2:0.2:0.9.

Reaction of $[H_3Ru_3(COMe)(CO)_6(PPh_3)_3]^{1+}$ with $[H_3Ru_3(COMe)(CO)_7(PPh_3)_2]^{1+}$ and PPh_3. In one 50 mL Schlenk flask was placed $H_3Ru_3(COMe)(CO)_6(PPh_3)_3$ (16.6 mg, 12.7 μmol), PPh_3 (3.7 mg, 14.4 μmol), and dichloromethane (10 mL), and in a second flask $H_3Ru_3(COMe)(CO)_7(PPh_3)_2$ (14.9 mg, 13.9 μmol) and dichloromethane (10 mL) were placed. To each flask was added $FeCp_2PF_6$ (4.7 mg (14.2 μmol) and 5.2 mg (15.7 μmol), respectively). Then the contents of the second flask were transferred via pipet to the first flask. The IR spectrum of the resulting solution displayed absorptions at 2080 m, 2072 m br, 2027 s, 2017 vs, and 1964 m cm^{-}.[1] After 15 min, the solution was evaporated to dryness. The ^1H NMR spectrum displayed resonances at −11.1, −11.5, and −12.3 ppm assigned to $[H_3Ru_3(CO)_7(PPh_3)_3]^{1+}$ (relative intensity 0.54), −15.75 and −16.35 ppm assigned to $H_3Ru_3(COMe)(CO)_7(PPh_3)_2$ (relative intensity 0.15), −12.9 (br, 1 H) and −16.65 (br, 1 H), unidentified (relative intensity 0.22), and −17.01 assigned to $[HRu_3(CO)_9(PPh_3)_3]^{1+}$ (relative intensity 0.09).

Two-Electron Oxidation of $H_3Ru_3(COMe)(CO)_{9-n}(PPh_3)_n$. When 2 equiv of $AgBF_4$ was added to the dichloromethane solution of $H_3Ru_3(COMe)(CO)_7(PPh_3)_2$, the solution turned into dark green and then dark red within minutes. Bulk electrolysis at the potential of the second oxidation also gave the same product, based on IR spectroscopy. The CO stretching frequencies shifted to higher values. The ^1H NMR spectrum displays hydride resonances at −17.24 (dd) ppm, with phosphorus−hydride coupling constants of 20.8 and 8.4 Hz, and −13.19 (d) ppm, with a phosphorus−hydride coupling constant of 10.4 Hz. The resonance assigned to a methoxy group appears at 4.53 ppm. In the ^{31}P NMR spectrum, two singlets at 38.1 and 28.1 ppm were observed. The product of the two-electron oxidation is proposed to be $[H_2Ru_3(COMe)(CO)_8(PPh_3)_2]^+$. This cation can be prepared by the alternative route of protonation of $HRu_3(COMe)(CO)_8(PPh_3)_2$.

Treatment of $H_3Ru_3(COMe)(CO)_6(PPh_3)_3$ with 2 equiv of $AgBF_4$ caused decomposition, and no products were identifiable. However, oxidation with 2 equiv of $FeCp_2PF_6$ in the presence of 1 equiv of PPh_3 generates $[H_3Ru_3(CO)_7(PPh_3)_3]^{1+}$.

Protonation of $HRu_3(\mu\text{-}COMe)(CO)_{10-n}(PPh_3)_n$ (n = 1−3). A mixture of clusters $HRu_3(COMe)(CO)_{10-n}(PPh_3)_n$ (n = 1−3) was prepared in cyclohexane.[16] The ratio of the products was controlled by the amount of PPh_3 for the ligand substitution reaction. Typically, three phosphine-substituted clusters, e.g., n = 1−3, can be obtained with a ratio of 2:2:1 by adding 2.5 equiv of PPh_3 and stirring overnight. Cyclohexane was removed by rotary evaporation. The residue was dried in vacuo and dissolved in $CDCl_3$ in a NMR tube. A ^1H NMR spectrum was recorded to determine the ratio of products. Then the solution was shaken vigorously after addition of an excess of CF_3COOH (5−8 μL) or CF_3SO_3H. The hydride signal due to the trisubstituted cluster disappeared immediately, giving rise to a very small signal at −17.36 ppm (d, J 3 Hz). After the solution was allowed to stand overnight, the ^1H NMR spectrum indicated that the protonation of the disubstituted cluster was complete, while the monosubstituted cluster remained unreacted. The protonation of $HRu_3(COMe)(CO)_8(PPh_3)_2$ was indicated clearly by ^1H NMR spectroscopy. The growth of new signals (−17.24 ppm, dd, 1H, J_{PH} = 20.8, 8.4 Hz; −13.19 ppm, d, 1H, J_{PH} = 10.4 Hz) due to the protonation product $[H_2Ru_3(COMe)(CO)_8(PPh_3)_2]^+$ were accompanied by diminution of the hydride signal due to the starting material $HRu_3(COMe)(CO)_8(PPh_3)_2$.

Oxidation of $H_3Os_3(COMe)(CO)_8(PPh_3)$. To a solution of 30 mg of $H_3Os_3(COMe)(CO)_8(PPh_3)$ in dichloromethane was added 7 mg (1 equiv) of AgO_3SCF_3. The solution turned green. After the mixture was stirred overnight, the color had changed to yellow-orange. The ^1H NMR spectrum of the products showed the presence of $[H_3Os_3(CO)_9(PPh_3)]^+$, starting material, and other unidentified products. The mixture was dissolved in MeOH (which deprotonates $[H_3Os_3(CO)_9(PPh_3)]^{1+}$). Thin-layer chromatography (silica gel, hexane elution) yielded $H_2Os_3(CO)_9(PPh_3)$ (10 mg, 34%).

Protonation of $H_2Os_3(CO)_{10}$ and $H_2Os_3(CO)_9(PPh_3)$. NMR samples of $[H_3Os_3(CO)_{10}]^{1+}$ and $[H_3Os_3(CO)_9(PPh_3)]^{1+}$ were prepared as previously reported.[18] NMR data for $[H_3Os_3(CO)_{10}]^{1+}$ ($CDCl_3$). ^{13}C NMR: 151.8 (2 C(a), d, J_{CH} 14.6 Hz), 164.4 (1 C(b), d, J_{CH} 4.0 Hz), 166.8 (1 C(c)), 170.1 (1 C(d)), 170.2 (1 C(e)), 170.5 (2 C(f)), 172.0 (2 C(g), d, J_{CH} 11.0 Hz) ppm. ^1H NMR: −12.33 (2 H(a), d, J_{ab} 1.4 Hz), −14.49 (1 H(b), t, J_{ab} 1.4 Hz) ppm. NMR data for $[H_3Os_3(CO)_9(PPh_3)]^{1+}$ ($CDCl_3$). ^{13}C NMR: 165.4 (1 C(a), d, J_{CH} 4 Hz), 165.7 (1 C(b), dd, J_{CH} 10 Hz, J_{CP} 9 Hz), 166.1 (1 C(c)), 168.0 (1 C(d), dd, J_{CH} 13 Hz, J_{CP} 10 Hz) 170.6 (1 C(e), d, J_{CH} 9 Hz), 170.7 (1 C(f)), 171.2 (1 C(g)), 173.6 (1 C(h), d, J_{CH} 13 Hz), 175.0 (1 C(i), dd, J_{CH} 10 Hz, J_{CP} 10 Hz) ppm. ^1H NMR: −11.89 (1 H (a), d, J_{aP} 7.3 Hz), −12.03 (1 H (b), J_{bP} 30.5 Hz), and −13.78 ppm (1 H(c), d, J_{cP} 9.3 Hz) ppm.

Electrochemistry. Cyclic voltammetric experiments were performed with Bioanalytical Systems, Inc. (West Lafayette, IN) instrumentation (BAS-100 and BAS-100W electrochemical analyzers). Measurements were made in accordance with standard techniques, which included purging of solutions with nitrogen to exclude oxygen. Dichloromethane was freshly distilled from calcium hydride and stored under nitrogen. The supporting electrolyte was 0.1 M tetrabutylammonium tetrafluoroborate, TBATFB (Kodak, also prepared by ion exchange of tetrabutylammonium bromide with sodium tetrafluoroborate), which had been recrystallized 3 times from ethanol/water and vacuum-dried. The working electrode for the experiments at relatively low scan rates was a platinum disk electrode (diameter = 3 mm). For work at higher scan rates and for some of the steady-state investigations, smaller platinum disks (BAS, diameter = 100 and 10 μm) were employed. A platinum wire served as the auxiliary (counter) electrode. The concentration of the analyte was 10^{-3} M unless stated otherwise. The reference electrode used was either the saturated calomel electrode (SCE) or Ag|AgCl|LiCl(satd) in C_2H_5OH. For voltammetric studies that involved relatively high scan rates, a quasi-reference electrode (silver wire) was employed. Compensation for resistive losses ("iR drop") was employed for all measurements. Under typical experimental conditions, the reversible oxidation for ferrocene was centered on E = 0.53 V vs SCE. The potential peak-to-peak separation, $\Delta E_p = E_{p,a} - E_{p,c}$, was within a range of 65 ± 5 mV. All potentials are reported relative to the ferrocene/ferricinium couple as 0 V. Simulated cyclic voltammograms were computed by means of DigiSim 2.1 software, obtained from Bioanalytical Systems, Inc. Details of the procedures followed are provided under Results and Discussion.

The diffusion coefficient for $H_3Ru_3(CNMeBz)(CO)_6(PPh_3)_3$ was determined to be $1.61(38) \times 10^{-6}$ cm^2 s^{-1} by using normal pulse voltammetry and linear regression of $(i_d 2\pi)/(nFAC_R^*)^2$ vs $1/t_p$ for experiments at a number of pulse widths (5, 50, 100 ms).[26] Assuming that the diffusion coefficients of the other clusters are similar to the value for the diffusion coefficient of $H_3Ru_3(CNMeBz)(CO)_6(PPh_3)_3$, the number of electrons, n, involved in the first oxidation process can be calculated from the cathodic peak current. For example, from the cyclic voltammetric data for $H_3Ru_3(COMe)(CO)_6(PPh_3)_3$, the cathodic peak current and the Randles−Sevcik equation gives n = 1.04.[21]

Controlled Potential Coulometry of $H_3Ru_3(CNMeBz)(CO)_6(PPh_3)_3$. The coulometric cell was assembled as follows: To a jacketed cell, kept at constant temperature (22 °C), was added 25 mL of a 0.1 M TBATFB solution of dichloromethane and 11.0 mg (7.89×10^{-6} moles) of $H_3Ru_3(CNMeBz)(CO)_6(PPh_3)_3$. A silver wire was used as a quasi-reference electrode, and a platinum wire served as the auxiliary electrode. Both electrodes made contact with the solution through fritted disks. The working electrode was a platinum gauze electrode (Aesar Unimesh, gauze type 39/1, 25 mm diameter × 50 mm height cylinder), placed directly into the solution. A cyclic voltammogram was performed prior to the coulometry to determine the correct potential. The solution was stirred vigorously and purged with nitrogen while the experiment was performed. After approximately 145 min, the current had decayed to background levels and the experiment was halted. The amount of charge passed was 0.73 C, and the value calculated for n, the number of electrons, was 0.96.

Results and Discussion

$H_3Ru_3(\mu_3\text{-}CX)(CO)_{9-n}L_n$. The syntheses and characterizations of a number of substituted clusters $H_3M_3(\mu_3\text{-}CX)(CO)_{9-n}L_n$ (M = Ru, X = OMe, L = $AsPh_3$, PPh_3, n = 1−3; M = Ru, X = SEt, Ph, NMeBz, L = PPh_3, n = 3; M = Os, X = OMe, L = PPh_3, n = 1, 2) have been described previously. The EPh_3 ligands occupy the axial coordination sites, trans to the Ru−CX bonds, e.g., $H_3Ru_3(CPh)(CO)_7(ax\text{-}AsPh_3)_2$.[15] For small ligands, pyridine and NCMe, equatorial coordination, cis to the Ru−CX bonds, is preferred.[22] We have now prepared the mixed substitution products $H_3Ru_3(COMe)(CO)_6(PPh_3)_2L$ (L = $P(OMe)_3$ and $CNCH_2Ph$) which exist in solution as equilibrium mixtures of $H_3Ru_3(COMe)(CO)_6(ax\text{-}PPh_3)_2(ax\text{-}L)$ and $H_3Ru_3(COMe)(CO)_6(ax\text{-}PPh_3)_2(eq\text{-}L)$, eq/ax = 2.8 and 7.3, respectively (Figure 1). We have also determined that this equilibrium exists for $H_3Ru_3(COMe)(CO)_6(PPh_3)_3$ (eq/ax = 0.15 in dichloromethane). Because of ring strain, $H_3Ru_3(COMe)(CO)_7(\mu\text{-}(PPh_2)_2CHPPh_2)$ is equatorially substituted but $H_3Ru_3(COMe)(CO)_6\{\mu_3\text{-}(PPh_2CH_2)_3CMe\}$ is axially substituted.[10b] The coordination geometry is easily established by ^{1}H NMR spectroscopy. Representative NMR and IR data are given in Tables 1 and 2, respectively; data for all compounds are reported in the Supporting Information (Tables 1S and 2S).

Electrochemistry. The electrochemical oxidations of the clusters $(\mu\text{-}H)_3Ru_3(\mu_3\text{-}CX)(CO)_{9-n}L_n$ are all chemically irreversible in acetonitrile, most likely because of the nucleophilic attack by the solvent on the oxidized species. For the monosubstituted clusters, the cyclic voltammetry for the oxidation is also chemically irreversible in dichloromethane. Anodic peak potentials, from cyclic voltammograms recorded at a scan rate of 100 mV/s, are given in Table 3. By contrast, cyclic voltammograms for dichloromethane solutions of disubstituted and trisubstituted clusters exhibit two oxidation responses, the first of which is either electrochemically reversible or quasi-reversible at scan rates of ca. 100 mV/s. The second process, at more positive potentials, is either quasi-reversible or irreversible and has not been examined in detail. Figure 2 shows a cyclic voltammogram for $H_3Ru_3(\mu_3\text{-}CSEt)(CO)_6(AsPh_3)_3$, which displays an electrochemically reversible first oxidation and a near-reversible second oxidation. Reversibility was assessed by comparing the values of the peak current ratio ($i_{p,c}/i_{p,a}$) and peak-to-peak separation (ΔE_p) for a scan rate of 100 mV/s with those for the ferrocene/ferricenium couple under the same conditions ($i_{p,c}/i_{p,a}$ = 1; $\Delta E_p = 65 \pm 5$ mV). Electrochemical data for the cluster series $H_3Ru_3(\mu_3\text{-}CX)(CO)_{9-n}(L)_n$ (n = 1−3) are collected in Table 3. For $H_3Ru_3(\mu_3\text{-}CNMeBz)(CO)_6(PPh_3)_3$, the first one-electron oxidation process is essentially electrochemically reversible at a scan rate of 100 mV/s (Figure 3a). Controlled potential coulometry performed on $H_3Ru_3(\mu_3\text{-}CNMeBz)(CO)_6(PPh_3)_3$ yielded a value of 0.96 F/mol for the first oxidation process.

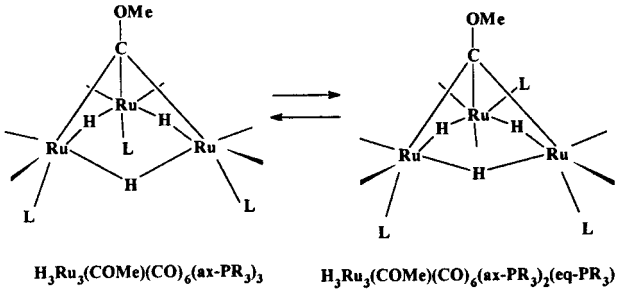

$H_3Ru_3(COMe)(CO)_6(ax\text{-}PR_3)_3$ $H_3Ru_3(COMe)(CO)_6(ax\text{-}PR_3)_2(eq\text{-}PR_3)$

Figure 1. Structures of the isomers $H_3Ru_3(\mu_3\text{-}COMe)(CO)_6(ax\text{-}L)_2(ax\text{-}L')$ and $H_3Ru_3(\mu_3\text{-}COMe)(CO)_6(ax\text{-}L)_2(eq\text{-}L')$.

For most of the other disubstituted and trisubstituted cluster compounds, however, the oxidation responses are best described as electrochemically quasi-reversible. This was confirmed by recording cyclic voltammetric responses over a range of scan rates. For most of the compounds, ΔE_p was found to increase with increasing scan rate while $i_{p,c}/i_{p,a}$ increased. The increase in $i_{p,c}/i_{p,a}$ indicates that a follow-up chemical process causes decomposition of the radical cation. In the present case, such a decomposition may involve reaction with the supporting electrolyte (TBATFB), as several of the oxidation products have long lifetimes in pure dichloromethane (the half-life is 1 h for decomposition of $[H_3Ru_3(\mu_3\text{-}COMe)(CO)_6(PPh_3)_3]^{1+}$). Other examples of electrolyte-induced decomposition have been reported.[23]

Chemical evidence (vide infra) indicates that for some of the clusters ligand isomerization, where a phosphine ligand migrates from an axial site to an equatorial site, accompanies the first oxidation process. In particular, $H_3Ru_3(\mu_3\text{-}CX)(CO)_6(PPh_3)_3$ (X = OMe and SEt) undergo this isomerization. Figure 3b shows a typical cyclic voltammogram for $H_3Ru_3(\mu_3\text{-}COMe)(CO)_6(PPh_3)_3$. Com-

(19) Bryan, E. G.; Jackson, W. G.; Johnson, B. F. G.; Kelland, J. W.; Lewis, J.; Schorpp, K. T. *J. Organomet. Chem.* **1976**, *108*, 385.
(20) For a more detailed account of the EPR experiment, see: Male, R.; Samotowka, M. A.; Allendoerfer, R. D. *Electroanalysis* **1989**, *1*, 333.
(21) (a) Bard, A. J.; Faulkner, L. R. *Electrochemical Methods*; John Wiley and Sons: New York, 1980. (b) Nicholson, R. S.; Shain, I. *Anal. Chem.* **1964**, *36*, 706.
(22) Beanan, L. R. Ph.D. Thesis, State University of New York at Buffalo, Buffalo, NY, 1986.

Table 1. ^{1}H and ^{31}P NMR Data in $CDCl_3$ Solution[a]

cluster	^{1}H NMR (ppm)	^{31}P NMR (ppm)
$H_3Ru_3(COMe)(CO)_6(ax\text{-}PPh_3)_3$	4.00 (s, 3H)	22.0
	−15.14 (t, 3H, J_{PH} = 7.7 Hz)	
$H_3Ru_3(COMe)(CO)_6(ax\text{-}PPh_3)_2(eq\text{-}PPh_3)$	−15.54 (br, 1 H)	
	−15.94 (br d, 1 H, J_{PH} ca. 40Hz)	
	−16.24 (br, 1 H)	
	3.69 (s, 3 H)	
$H_3Ru_3(CNMeBz)(CO)_6(PPh_3)_3$	2.93 (s, 3H)	22.1
	4.51 (s, 2H)	
	−15.11 (t, 3H, J_{PH} = 6.3 Hz)	
$H_3Ru_3(CSEt)(CO)_6(PPh_3)_3$	4.08 (t, 3H, J_{HH} = 7.1 Hz)	23.0
	3.32 (q, 2H)	
	−15.33 (t, 3H, J_{PH} = 7.6 Hz)	
$[H_3Ru_3(COMe)(CO)_6(PPh_3)_3]^{1+}$	4.1 (v br)	
	−15.1 (v br)	
$[H_3Ru_3(COMe)(CO)_6(AsPh_3)_3]^{1+}$	4.0 (v br)	
	−15.2 (v br)	
$[H_3Ru_3(COMe)(CO)_7(PPh_3)_2]^{1+}$	3.9 (v br)	
	−15.8, −16.4 (v br)	
$[H_3Ru_3(CSEt)(CO)_6(PPh_3)_3]^{1+}$	3.5, 1.4 (v br)	
	−15.6 (v br)	
$[H_3Ru_3(CNMeBz)(CO)_6(PPh_3)_3]^{1+}$	9.2−8.8 (v br)	
	6.0, 5.2 (v br)	
	hydride not observed	
$H_3Ru_3(COMe)(CO)_6(PPh_3)_2(CNBz)$ isomer I, axial CNBz	−16.06 (dd, 2H, J_{PH} = 12.2 Hz, J_{HH} = 2 Hz),	22.0 (s)
	−15.72 (tt, 1H, J_{PH} = 11.3 Hz, J_{HH} = 2 Hz)	
	4.53 (s, 2H)	
	3.95 (s, 3H)	
$H_3Ru_3(COMe)(CO)_6(PPh_3)_2(CNBz)$ isomer II, equatorial CNBz	−16.92 (d, 1H, J_{PH} = 11.7 Hz)	22.5 (s, 1P)
	−16.53 (d, 1H, J_{PH} = 11.1 Hz)	21.3 (s, 1P)
	−15.72 (t, 1H, J_{PH} = 11.3 Hz)	
	4.70 (d, 1H, J_{HH} = 17.0 Hz)	
	4.78 (d, 1H, J_{HH} = 17.0 Hz)	
	3.95 (s, 3H)	
$H_3Ru_3(COMe)(CO)_6(PPh_3)_2(P(OMe)_3)$ isomer I, equatorial $P(OMe)_3$	−16.71 (ddt, 1 H, J_{HH} 2 Hz, J_{PH} 10.6, 15.9 Hz)	
	−16.06 (br t, 1 H, J_{PH} ca. 8.5 Hz)	
	−15.81 (br t, 1 H, J_{PH} ca. 9 Hz)	
	3.44 (d, 9 H, J_{PH} 12 Hz)	
	3.97 (s, 3 H)	
$H_3Ru_3(COMe)(CO)_6(PPh_3)_2(P(OMe)_3)$ isomer II, axial $P(OMe)_3$	ca. −15.9 (2 H, obscured)	
	−15.65 (br t, 1 H, J_{PH} 9.5 Hz)	
	3.27 (d, 9 H, J_{PH} 12 Hz)	
	4.02 (s, 3 H)	
$[H_3Ru_3(CO)_7(PPh_3)_3]^{1+}$	−11.13 (br s, 1H)	29.4 (1P)
	−11.56 (d, 1H, J_{PH} = 48 Hz)	33.7 (1P)
	−12.35 (br s, 1H)	40.4 (d, 1P,
$[H_3Ru_3(CO)_6(CS)(PPh_3)_3]^{1+}$	−11.07 (br s, 1H)	J_{PH} = 48 Hz)
	−11.50 (d, 1H, J_{PH} = 45 Hz)	
	−12.29 (br s, 1H)	
$[H_3Ru_3(CO)_7(AsPh_3)_3]^{1+}$	−10.96 (m, 1H)	
	−12.49 (m, 1H)	
	−12.59 (m, 1H)	

[a] Phenyl resonances are not reported.

Table 2. IR Data for Selected $[(\mu\text{-}H)_3Ru_3(\mu_3\text{-}CX)(CO)_{9-n}L_n]^{0/1+}$ in Dichloromethane

cluster	ν(CO), cm^{-1}
$H_3Ru_3(COMe)(CO)_6(PPh_3)_3$	2035 s, 2010 vs, 1959 m
$H_3Ru_3(CNMeBz)(CO)_6(PPh_3)_3$	2031 s, 2005 s br, 1953 m
$H_3Ru_3(CSEt)(CO)_6(PPh_3)_3$	2036 s, 2013 vs, 1963 m
$[H_3Ru_3(COMe)(CO)_6(PPh_3)_3]^{1+}$	2069 w sh, 2062 w, 2045 vs, 2037 sh, 2007 s, 1961 w
$[H_3Ru_3(CNMeBz)(CO)_6(PPh_3)_3]^{1+}$	2057 s, 2036 vs, 1993 s
$[H_3Ru_3(CSEt)(CO)_6(PPh_3)_3]^{1+}$	2085 vw, 2065 m, 2044 vs, 2036 vs, 2028 m, 2014 vs, 2005 s, 1992 w, 1964 w
$H_3Ru_3(COMe)(CO)_6(CNBz)(PPh_3)_2$	2178 w, 2030 m, 2011 vs, 2001 sh, 1967 m, 1954 m, 1939 sh
$H_3Ru_3(COMe)(CO)_6(P(OMe)_3)(PPh_3)_2$	2036 m, 2032 m, 2011 vs, 2002 m sh, 1964 m, 1954 m

parison of this response with that of Figure 3a (for the μ_3-CNMeBz analog) shows a significantly larger value of ΔE_p for the former. While such an increase in this parameter may be due simply to slower electron-transfer kinetics, it is also consistent with the ECEC mechanism. Here, the electrochemical behavior is described by the so-called "square" reaction scheme (Scheme 1). The behavior that follows this scheme has been noted for a number of organometallic redox processes.[1f]

Further support for the presence of a mechanism that involves both chemical and electrochemical steps was obtained by a more extensive examination of the cyclic voltammetric responses over a range of potential scan rates. To minimize the distortion of responses due to the effects of uncompensated solution resistance, vol-

Table 3. Cyclic Voltammetric Data for $H_3Ru_3(\mu_3\text{-}CX)(CO)_{9-n}L_n$ ($n = 1-3$) in Dichloromethane[a]

cluster	$(E_{p,a} + E_{p,c})/2$ [$E_{p,a1}$] (V)	ΔE_p (mV)	$i_{p,c}/i_{p,a}$	$E_{p,a2}$ (V)
$H_3Ru_3(COMe)(CO)_9$	[0.53]			
$H_3Ru_3(COMe)(CO)_8(PPh_3)$	[0.29]			
$H_3Ru_3(COMe)(CO)_7(PPh_3)_2$	−0.02	70	0.88	0.24
$H_3Ru_3(COMe)(CO)_6(PPh_3)_3$	−0.22	95	0.77	0.07
$H_3Ru_3(COMe)(CO)_6(PPh_3)_2(P(OMe)_3)$	−0.24	72	0.97	0.08
$H_3Ru_3(COMe)(CO)_6(PPh_3)_2(CNCH_2Ph)$	−0.19	72	0.93	0.13
$H_3Ru_3(COMe)(CO)_8(AsPh_3)$	[0.37]			
$H_3Ru_3(COMe)(CO)_7(AsPh_3)_2$	0.10	74	0.78	0.34
$H_3Ru_3(COMe)(CO)_6(AsPh_3)_3$	−0.08	86	0.84	0.15
$H_3Ru_3(CNMeBz)(CO)_6(PPh_3)_3$	−0.59	61	0.97	−0.18
$H_3Ru_3(CNMeBz)(CO)_6(SbPh_3)_3$	−0.37	68	0.91	0.08
$H_3Ru_3(CSEt)(CO)_6(PPh_3)_3$	−0.18	77	0.78	0.28
$H_3Ru_3(CSEt)(CO)_6(AsPh_3)_3$	−0.09	72	0.83	0.29
$H_3Ru_3(CPh)(CO)_6(PPh_3)_3$	0	74	0.93	0.50
$H_3Ru_3(CMe)(CO)_6(PPh_3)_3$	0	73	0.91	0.42
$H_3Ru_3(CEt)(CO)_6(PPh_3)_3$	−0.01	74	0.93	0.45
$H_3Ru_3(CBr)(CO)_6(PPh_3)_3$	0.22	120	0.76	0.68
$H_3Ru_3(COMe)(CO)_6\{(PPh_2CH_2)_3CEt\}$	−0.11	81	0.60	0.10
$H_3Ru_3(COMe)(CO)_7\{(PPh_2)_2CHPPh_2\}$	[0.12]			
$H_3Os_3(COMe)(CO)_9$	[0.54]			
$H_3Os_3(COMe)(CO)_8(PPh_3)$	[0.31]			
$H_3Os_3(COMe)(CO)_7(PPh_3)_2$	−0.01	85	0.66	0.27

[a] Cluster (10^{-3} M) in 0.1 M TBATFB in dichloromethane. The working electrode was a 5 mm diameter platinum disk, and the auxiliary electrode was a platinum wire. The reference electrode was either a silver wire or SCE. The scan rate was 100 mV/s. The potentials are referenced to the ferrocene/ferricenium couple (0 V, $\Delta E_p = 72$ mV) under the same conditions.

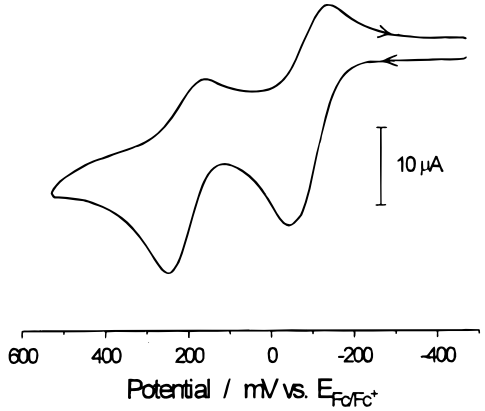

Figure 2. Cyclic voltammogram for $H_3Ru_3(\mu_3\text{−}CSEt)(CO)_6(AsPh_3)_3$.

tammograms were recorded at a working electrode of relatively small dimensions (platinum disk, diameter = 100 μm). Use of this electrode, together with a platinum-wire quasi-reference electrode, allowed essentially full compensation for resistive losses. From this basis, it was then possible to attribute any changes in peak position and/or peak-to-peak separation to the influence of kinetic (chemical and electrochemical) parameters.

Figure 4 shows typical cyclic voltammetric responses for the first oxidation process of $H_3Ru_3(\mu_3\text{-}COMe)(CO)_6(PPh_3)_3$ in dichloromethane solution, for scan rates from 1 to 100 V/s. At 1 V/s (Figure 4a), it is clear that the oxidation step for this compound is not a simple process. The response for oxidation on scanning toward more positive potentials is followed on the reverse scan by two reduction processes. These are separated by ∼100 mV. Comparison with Figure 3b, recorded at a scan rate of 100 mV/s, suggests that the single reduction process observed at the lower scan rate coincides with the process at the more negative potential in Figure 4a. The general shape of the latter response is consistent with one of the well-known ECE systems, where a

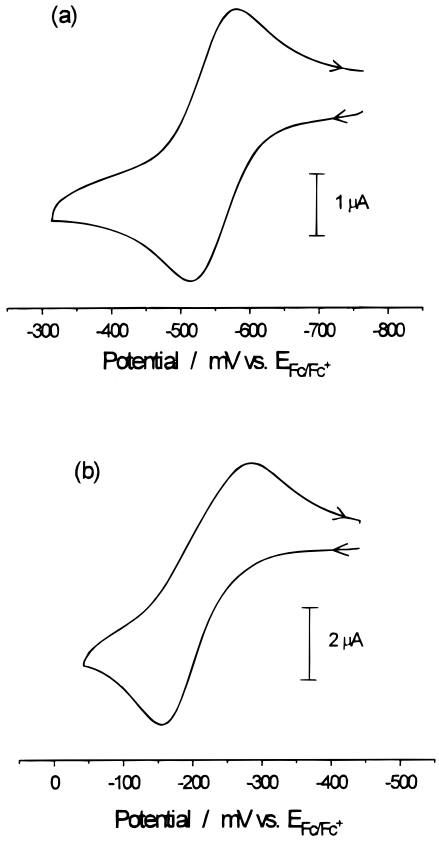

Figure 3. Cyclic voltammogram for the first oxidation of (a) $H_3Ru_3(\mu_3\text{−}CNMeBz)(CO)_6(PPh_3)_3$ and (b) $H_3Ru_3(\mu_3\text{−}COMe)(CO)_6(PPh_3)_3$ at 100 mV/s.

chemical reaction (C) follows an electrochemical step (E) and yields a product that is also electroactive (second E).

In fact, the oxidation response for $H_3Ru_3(\mu_3\text{-}COMe)(CO)_6(PPh_3)_3$ involves a second oxidizable species. This becomes apparent when two cycles through the potential range are completed (Figure 4b). Now the response is consistent with two redox processes, separated by ∼100

Scheme 1

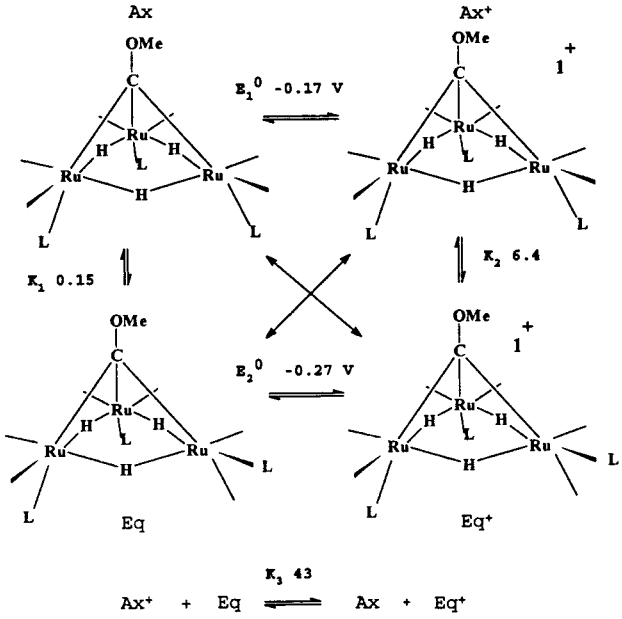

mV, for which all four participating species are stable on the time scale of the potential sweep. This situation fits well with the spectroscopic data that show these compounds are prone to undergo isomerization between so-called "axial" and "equatorial" forms. Given that the dominant form of the neutral compound in bulk dichloromethane solution is the axial (Ax) isomer, the oxidation−reduction pair at the more positive potential is assigned to the couple Ax−Ax$^+$, where Ax$^+$ represents the corresponding cationic species. The second redox pair is due to the equatorial form (neutral species and cation, Eq−Eq$^+$).

According to the general representation for the ECEC system (Scheme 1), the influence of the kinetic parameters for the two isomerization reactions (k_1, k_{-1}, k_2, and k_{-2}) is revealed by the dependence of the cyclic voltammetric responses on scan rate. As shown in Figure 4c, increasing the scan rate (to 5 V/s) causes a change in the response as the current due to the reduction process for Eq$^+$ becomes smaller. At 100 V/s (Figure 4d), the cyclic voltammogram consists almost exclusively of responses for the Ax−Ax$^+$ couple. (In fact, a response for the Eq couple would be expected at this scan rate, due to the small amount of this isomer present in the bulk solution. As shown below, however, broadening of the Eq response (due to the encroachment of electrochemical kinetic effects) causes this response to disappear into the large background (charging) current.) Further characterization of the kinetic parameters for Scheme 1 was undertaken through simulation of the voltammetric responses with DigiSim (v. 2.1). Data for $H_3Ru_3(\mu_3\text{-COMe})(CO)_6(PPh_3)_3$ were used as the basis for the simulation.

Estimates of the values for the input parameters were derived from the electrochemical and spectroscopic studies. As noted above, careful choice of the electrode size and instrument settings allowed effectively complete compensation for the effects due to solution resistance. Consideration of the latter, along with the cell time constant, also provided a good estimate for the double layer capacitance. Hence, simulated voltammograms feature charging currents that are of the same order as those for the experimental counterparts. From the ^{1}H NMR spectra, recorded for dichloromethane-d_2 solutions, integration of the hydride resonances provided $K_1 = 0.15$. An initial value for the equilibrium constant (K_2) for the interconversion of Ax$^+$ and Eq$^+$ was obtained from voltammetric studies on a solution of $H_3Ru_3(\mu_3\text{-COMe})(CO)_6(PPh_3)_3$ that had been treated with 1 equiv of $AgBF_4$ (vide infra). Oxidation with Ag^+ produces solutions in which the predominant form of the cationic species is the equatorial isomer (Eq$^+$). An analysis of the voltammetric responses suggested a value for [Eq$^+$]/[Ax$^+$] of around 6. Ultimately, the lack of accuracy in the estimation of K_2 had no effect on the quality of the simulation of Scheme 1 for $H_3Ru_3(\mu_3\text{-COMe})(CO)_6(PPh_3)_3$. Indeed, close fitting of simulated and experimental data provided an accurate estimate for $\Delta E°$ (the difference in the potentials for the Ax and Eq couples) which, in combination with K_1, fixes the value of K_2, on thermodynamic grounds.

The general applicability of the ECEC mechanism was tested by making a series of relatively coarse adjustments to the least-well-defined of the input parameters. Having obtained a good qualitative correspondence between the experimental and computed voltammograms, the fitting routine of DigiSim was utilized to refine the parameter set. The results are shown in Figure 5, parts of which may be compared with the corresponding voltammograms in Figure 4. An important feature of the simulation, that is not evident in Figures 4 and 5, is the dependence of the cyclic voltammetric responses on the concentration of the cluster. Comparison of the responses obtained for 1 and 10 mM solutions showed slightly less current for the reduction of Eq$^+$ at the higher concentration. This observation is consistent with the effects of the "cross-reaction" defined in Scheme 1. Second-order rate constants for this reaction were obtained by conducting a further series of simulations for analyte concentrations set at 1 and 10 mM. As a result, the final parameter set provides an accurate description of the electrochemical behavior over at least one order of magnitude in concentration. Table 4 contains a summary of rate and equilibrium constants derived from the refined simulation.

Ligand and Substituent Effects Upon Oxidation Potential. The relationship between the structure of a molecule and its oxidation potential is one of the most fundamental of all chemical concepts. Correlations of oxidation potentials with substituent effects and with HOMO energies have been noted by a number of workers.[24,25] Ligand additivity, the postulate that the effect of a particular ligand upon the oxidation potential is a function of that ligand only and is independent of the other ligands of the complex, is a well-established concept for substituted mononuclear complexes, for which the HOMO usually has dπ character.[24] To date, ligand additivity in metal cluster systems has not been

(23) Paw, W.; Lake, C. H.; Churchill, M. R.; Keister, J. B. *Organometallics* **1995**, *14*, 3768.
(24) Bursten, B. E.; Green, M. R. *Prog. Inorg. Chem.* **1988**, *36*, 393 and references therein.
(25) Lever, A. B. P. *Inorg. Chem.* **1990**, *29*, 1271.
(26) Alexiou, A. D. P.; Toma, H. E. *J. Chem. Res., Synop.* **1993**, 464.
(27) Hansch, C.; Leo, A.; Taft, R. W. *Chem. Rev. (Washington, D.C.)* **1991**, *91*, 165.

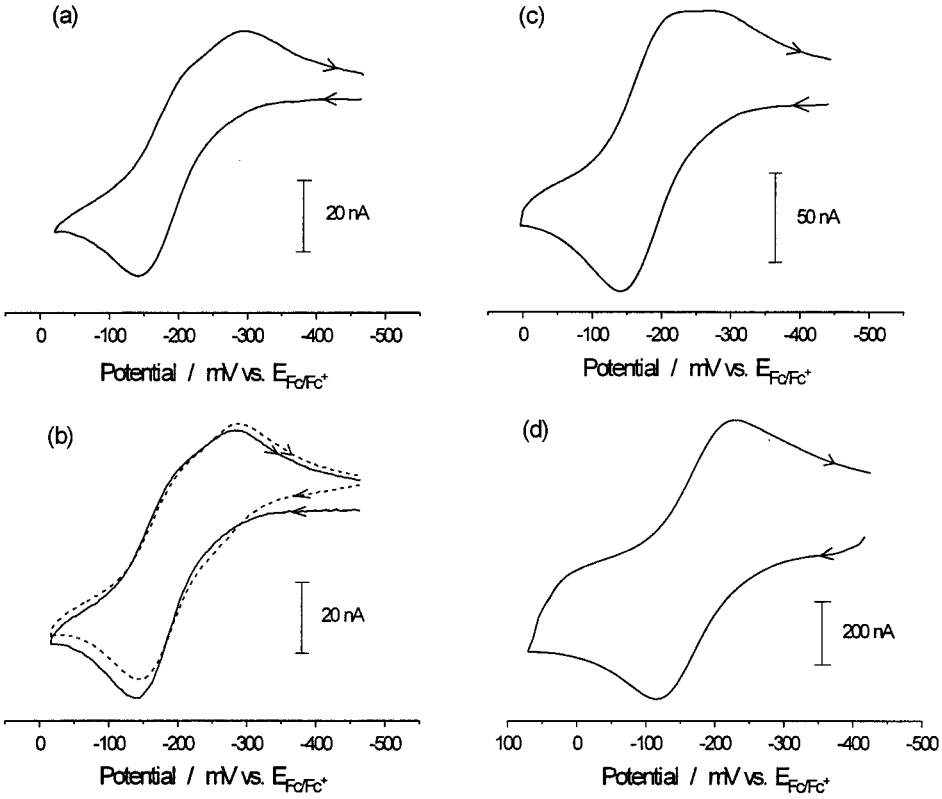

Figure 4. Cyclic voltammograms for 10^{-3} M $H_3Ru_3(\mu_3-COMe)(CO)_6(PPh_3)_3$ at scan rates of (a) 1 V/s; (b) 1 V/s, — first cycle, - - - second cycle; (c) 5 V/s; (d) 100 V/s.

investigated in a systematic manner. The electrochemistry of the series $(\mu\text{-H})_3Ru_3(\mu_3\text{-CX})(CO)_{9-n}(L)_n$ provides valuable insight into ligand additivity and substituent effects in cluster systems. Here, we adopt the terminology that "ligand effects" refer to effects due to the steric and electronic properties of the ligand directly bonded to a metal center (e.g., CO vs PPh_3), whereas "substituent effects" are effects due to the steric and electronic properties of substituents of organic moieties remote from the metal center (e.g., substituents on the hydrocarbyl fragment).

A variety of parameter sets have been developed to correlate the various properties of the metal complexes with the steric and electronic properties of ligands such as tertiary phosphines. Lever has established a set of ligand parameters E_L based upon an extensive compilation of oxidation potentials for octahedral Ru(II)/Ru(III) mononuclear complexes.[25] This ligand parameter set allows for the prediction of $E_{1/2}$ for any given octahedral mononuclear Ru(II) complex. The most general expression for the oxidation potentials for octahedral complexes of other metals is given in eq 1, where I_M and S_M are characteristic for the metal couple.

$$E_{obsd}(V) = S_M[\sum_0^i a_i E_L(L_i)] + I_M \qquad (1)$$

One report of the application of the Lever parameters to a cluster has appeared. The oxidation potential of $[Ru_3(\mu_3\text{-O})(OAc)_6L_3]^n$ ($n = -1$ to $+2$) was studied by Toma.[26] This compound, which is a 51-e cluster in the +1 state, differs from the clusters described below because the HOMO is not associated with the organometallic cluster bonding framework (indeed there are no Ru—Ru bonds).

Linear free-energy relationships involving substituent effects are used extensively in organic and inorganic chemistry.[27] Many correlations involving σ_p or σ_p^+ have been reported. The former parameter is based upon the pK_a of para-substituted benzoic acids and does not involve conjugative interactions. The latter set is derived from rates of solvolysis of substituted cumyl chlorides and, therefore, reflects direct conjugation between the substituent and an electron-deficient center. One recent example is the correlation of the oxidation potentials of $(\eta^6\text{-}C_6H_5X)Cr(CO)_3$ with the substituent parameters.[28] The oxidation potentials of $Fe(\eta^5\text{-}C_5H_4X)Cp$ have also been subjected to analysis;[29] although the best correlation involves σ_P for most substituents, strong π donors appear to correlate better with the σ_p^+ values. Lever has correlated ligand-based redox potentials with σ_p values.[30]

It is enlightening to correlate the oxidation potentials for $(\mu\text{-H})_3Ru_3(\mu_3\text{-CX})(CO)_{9-n}(L)_n$ with the ligand parameters E_L and the substituent parameters for the hydrocarbyl ligand. Electrochemical one-electron oxidation of $(\mu\text{-H})_3Ru_3(\mu_3\text{-CX})(CO)_{9-n}(L)_n$ ($n = 2$ or 3) is a kinetically facile process. As the oxidations of the monosubstituted clusters are irreversible, we have used for comparison the anodic peak potentials as determined by cyclic voltammetry at 100 mV/s. It should be noted that $(E_{p,a} - E_{1/2})$ will increase as the couple becomes more irreversible, and therefore, comparisons of data for the quasi-reversible and irreversible examples should be viewed with caution. Also, we have a very limited variety of ligand and substituent types. Nonetheless,

(28) Hunter, A. D.; Mozol, V.; Tsai, S. D. *Organometallics* **1992**, *11*, 2251.
(29) Britton, W. E.; Kashyap, R.; El-Hashash, M.; El-Kady, M.; Herberhold, M. *Organometallics* **1986**, *5*, 1029 and references therein.

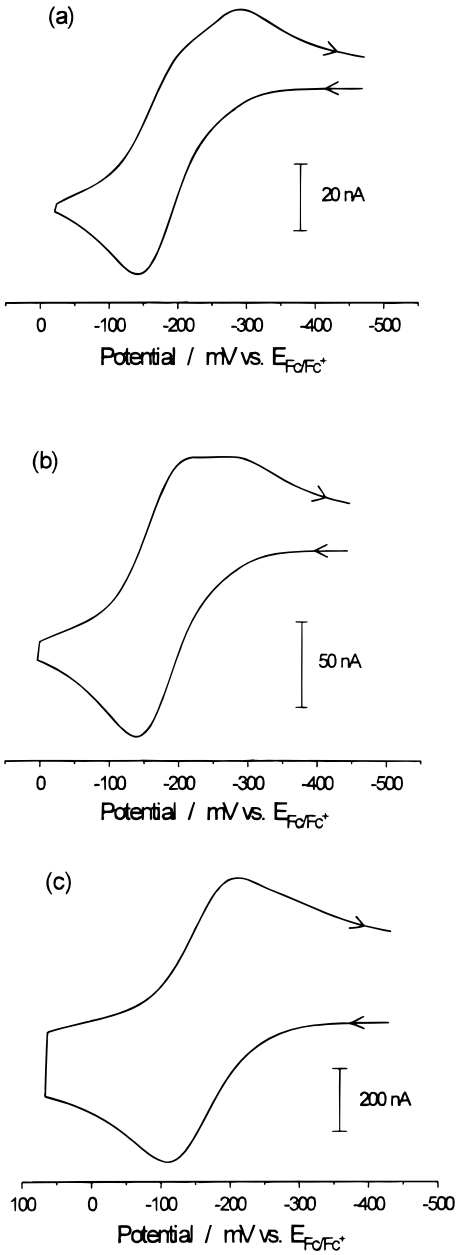

Figure 5. Computed cyclic voltammograms (DigiSim v. 2.1) for 10^{-3} M $H_3Ru_3(\mu_3-COMe)(CO)_6(PPh_3)_3$ at scan rates of (a) 1 V/s; (b) 5 V/s; (c) 100 V/s.

a good fit (S_{M3} = 0.37(0.03), ρ = 6.0(0.7), and I_{M3} = −2.5(0.2) V (correlation 0.962, Figure 6) of the observed anodic peak potentials (at 100 mV/s) can be made to eq 2.

$$E_{obsd}(V) = S_{M_3}\sum_{i=1}^{9} E_L(L_i) + 2.303(RT/nF)\rho\sigma^+_p(X) + I_{M_3} \quad (2)$$

Equation 2 is a modified version of Lever's[25] with inclusion of a Hammet term.[27] The correlation with the substituent parameters σ_p is much poorer than with σ_p^+, indicating that π conjugation is important in stabilizing the radical cation. The factor $2.303(RT/nF)$ is included to provide units of volts. Here, the ligand parameters E_L are summed over the CO or ER_3 ligands of the triruthenium core, and the substituent parameters are summed over the n hydrocarbyl substituents X_i, in this case the single methylidyne substituent. The constant I_{M3} serves to scale the potential to a hypothetical complex $H_3Ru_3(\mu_3-CH)L_9$ where $E_L(L) = 0$ and corrects for differences in reference potentials (Lever's E_L parameters are based upon the NHE reference, whereas we are using ferrocene/ferricenium = 0 V).

The coefficient ρ represents the sensitivity of the oxidation potential to the alkylidyne substituent. The π interaction is manifested in a very high value. The oxidation potentials of $Cr(\eta^6-C_6H_5X)(CO)_3$[28] and $Fe(\eta^5-C_5H_4X)Cp$[29] have been previously correlated with σ_I and σ_p, respectively. The nonlinear least-squares fits of the published oxidation potentials for $Cr(\eta^6-C_6H_5X)(CO)_3$ and $Fe(\eta^5-C_5H_4X)Cp$ to eq 2 (with $S_{M3} = 0$) with ring substituent constants σ_p^+ yield ρ = 3.8(0.3) (correlation 0.981) and 5.2(0.4) (correlation 0.975), respectively. Thus, the oxidation potential of the alkylidyne cluster core is even more sensitive to π-donor substituent effects than are the aromatic π complexes to substituents on the rings.

The bonding of $(\mu-H)_3Ru_3(\mu_3-CX)(CO)_9$ (X = H, Cl, and Br) has been the subject of a previous study. Fenske−Hall MO calculations performed by Sherwood and Hall[9] indicate that the HOMO for $H_3Ru_3(CX)(CO)_9$ (X = H, Cl, Br) is involved primarily in the Ru−C bonding interaction. The methylidyne carbon is best described as sp-hybridized with delocalized metal−carbon bonds, consisting of a weak bond involving the carbon "lone pair", and a stronger interaction with the carbon 2p orbitals. The HOMO for X = H is described as Ru−C "lone pair" antibonding. A pair of degenerate bonding orbitals which lie somewhat lower in energy is described as being formed from the Ru_3 $\{e_g^*\}$ and C $2p_\pi$ orbitals. However, for the π-donor substituents Cl and Br, the delocalization of the halogen lone pairs into the degenerate set makes these orbitals the HOMOs. For X = Ph, OMe, SEt, and NR_2, the lower symmetry will split the degeneracy but the description of the HOMO will be as for the halogen derivatives. When the methylidyne substituent is a strong π-donor group such as MeO, the electron pairs are strongly delocalized onto the cluster. Thus, it is not surprising that the oxidation potential of the cluster is strongly dependent upon the π-donor properties of X, in addition to the degree of phosphine substitution on the metal atoms.

The first term in eq 2 represents the effect of ligand substitution for CO upon the oxidation potential of the cluster. The coefficient S for a mononuclear Ru(II)/Ru(III) couple is ideally 1. The linearity of the fit, which includes clusters differing in the number of metal atoms which are substituted, indicates that each metal atom contributes equally to the HOMO. As for monometallic complexes, ligand additivity is conserved.[24] The value of S_{M3} = 0.37 indicates that delocalization over three Ru atoms reduces the dependence of the oxidation potential upon a ligand on any given Ru atom.

Substitution of each phosphine or arsine ligand for a carbonyl decreases the oxidation potential by approximately 150−200 mV per ligand. Surprisingly, there is a very significant difference in the donor properties of EPh_3, E = P > As ≥ Sb. Lever's E_L parameters are essentially the same for these (E = P (0.39), As (0.38), and Sb(0.38)). Other parameter sets also suggest similar electronic properties for these ligands.[31]

Table 4. Summary of Parameters for Simulation of Voltammograms

electron transfer	thermodynamics $E°'$	kinetics α	kinetics k_s
$Ax^+ + e^- \rightleftharpoons Ax$	+0.172 V ($E_1°$)	0.5	0.15 cm s^{-1}
$Eq^+ + e^- \rightleftharpoons Eq$	+0.267 V ($E_2°$)	0.5	0.10 cm s^{-1}

reaction isomerization	thermodynamics K	kinetics k_f	kinetics k_b
$Ax \rightleftharpoons Eq$	0.15 (K_1)	2.0×10^{-4} s^{-1}	1.3×10^{-3} s^{-1}
$Ax^+ \rightleftharpoons Eq^+$	6.44 (K_2)	6.5 s^{-1}	1.0 s^{-1}
$Ax^+ + Eq \rightleftharpoons Ax + Eq^+$	43.0 (K_3)	2×10^5 M^{-1} s^{-1}	4.7×10^3 M^{-1} s^{-1}

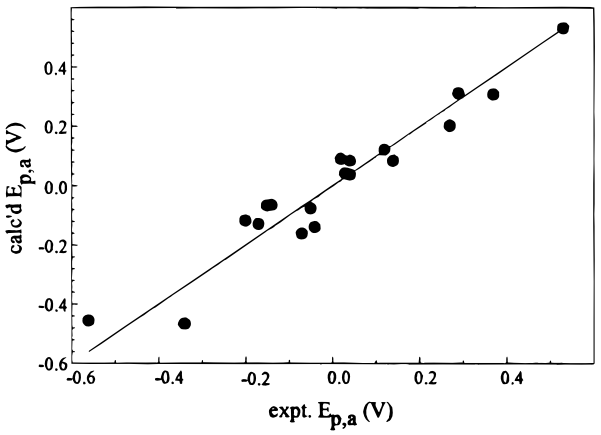

Figure 6. Correlation of experimental anodic peak potentials (at 100 mV/s), experimental $E_{p,a}$, vs potentials calculated, calculate $E_{p,a}$, from eq 2, with $S_{M3} = 0.37$, $\rho = 6.0$, and $I_{M3} = -2.5$ V.

There appears to be only a small dependence of the oxidation potential upon the geometry of the substitution product. The oxidation potential for $H_3Ru_3(COMe)(CO)_6(ax\text{-}PPh_3)_2(eq\text{-}PPh_3)$ is 95 mV less positive than that of $H_3Ru_3(COMe)(CO)_6(ax\text{-}PPh_3)_3$, and only one oxidation wave is found for $H_3Ru_3(COMe)(CO)_6(ax\text{-}PPh_3)_2(P(OMe)_3)$, which exists as a 3:1 mixture of equatorially and axially substituted isomers.

One-Electron Oxidations Using Chemical Reagents. As was the case with electrochemical oxidation, chemical oxidations in acetonitrile did not produce characterizable cluster products. However, in dichloromethane solution, a variety of oxidants, including $AgSO_3CF_3$, $AgBF_4$, $[FeCp_2]PF_6$, and $[Fe(o\text{-}phen)_3]^{3+}$, caused the color of the solution of the di- or trisubstituted cluster to change immediately from red-orange to dark green. The addition of Ag^+ to solutions of the cluster also leads to the formation of a silver mirror; exceptions are $H_3Ru_3(\mu_3\text{-}CR)(CO)_6(PPh_3)_3$ (R = Me, Ph) which undergo a parallel one-electron oxidation and formation of adducts with Ag^+. The nature of these adducts will be presented in a later paper. The oxidation products are proposed to be the 47-electron clusters $[H_3Ru_3(CX)(CO)_6(PPh_3)_3]^{1+}$; on the basis of the IR and EPR data (vide infra), these clusters are proposed to be isostructural with the 48-electron precursor, with all-axial PPh_3 ligands for X = Ph and NMeBz (C_{3v} symmetry) but one equatorial PPh_3 ligand and two axial PPh_3 ligands for X = OMe or SEt (C_1 symmetry).

To verify that the clusters remain intact upon chemical oxidation, two separate experiments were performed. The first was an electrochemical experiment. A cyclic voltammogram of $H_3Ru_3(COMe)(CO)_6(PPh_3)_3$ was recorded, then Ag^+ was added to the solution in the amounts of 0.25, 0.5, 0.75, and 1 equiv, each time recording the voltammogram. In each case, the voltammogram was unchanged, despite the fact that the solution had turned from orange to green. The second experiment involved oxidation of a solution of the cluster, followed by chemical reduction and a determination of the starting material recovered. A solution of $H_3Ru_3(COMe)(CO)_6(PPh_3)_3$ was oxidized with Ag^+. Dropwise addition of a THF solution of Na/benzophenone ketal caused the solution to turn from green to orange. TLC of this mixture and work up produced 93% of the starting material used. Thus, the integrity of the cluster is retained after oxidation.

The ^1H NMR spectrum for the green solution formed upon addition of 1 equiv of $AgSO_3CF_3$ or $FeCp_2PF_6$ to a solution of $H_3Ru_3(\mu_3\text{-}COMe)(CO)_6(PPh_3)_3$ displays broad resonances in the methyl (4 ppm) and hydride (−15 ppm) regions of the spectrum, which are indicative of the formation of a paramagnetic species, proposed to be the 47-electron radical cation $[H_3Ru_3(\mu_3\text{-}COMe)(CO)_6(PPh_3)_3]^{1+}$. A broad resonance is also observed in the ^{31}P NMR spectrum of this compound, centered at 20.9 ppm. Even when 0.5 equiv of oxidant is added, only these broad resonances are observed, suggesting rapid electron transfer between 47- and 48-electron clusters. In general, the same observations were made for all of the di- and trisubstituted clusters studied. However, because the stabilities of the oxidized clusters vary greatly, data could not be obtained for all of the 47-electron clusters. For each, the IR spectrum (Table 2) displays higher CO stretching frequencies than its 48-electron precursor, as expected for positively charged clusters. The IR spectrum for the oxidation product of $H_3Ru_3(CNMeBz)(CO)_6(PPh_3)_3$ displays the same pattern as the neutral precursor, suggesting a similar symmetry with three axial PPh_3 ligands. However, spectra for the oxidation products of $H_3Ru_3(COMe)(CO)_6(EPh_3)_3$ (E = As, P) display a higher number of bands, consistent with lower symmetry due to the presence of one equatorial and two axial PPh_3 ligands. IR and ^1H NMR data for the oxidized clusters are given in Tables 1 and 2.

The green solutions of the oxidized clusters were found to be EPR-active. Figure 7 shows the EPR spectrum for the radical cation $[H_3Ru_3(CNMeBz)(CO)_6(PPh_3)_3]^{1+}$, and Figure 8 shows the spectrum of $[H_3Ru_3(COMe)(CO)_6(PPh_3)_3]^{1+}$. The EPR data for each of the clusters are summarized in Table 5. A qualitative assessment of the stability of the radical cations can be made from the observation of the persistence of the green solution and the decay of the EPR signal with

(30) Masui, H.; Lever, A. B. P. *Inorg. Chem.* **1993**, *32*, 2199.
(31) (a) Brown, T. L.; Lee, K. J. *Coord. Chem. Rev.* **1993**, *128*, 89. (b) Tolman, C. A. *Chem. Rev. (Washington, D.C.)* **1977**, *77*, 313.

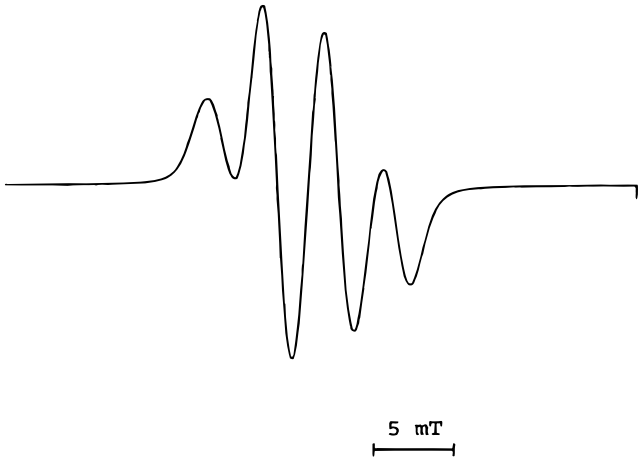

Figure 7. EPR spectrum for $[H_3Ru_3(\mu_3-CNMeBz)(CO)_6(PPh_3)_3]^{1+}$ in dichloromethane at 20 °C.

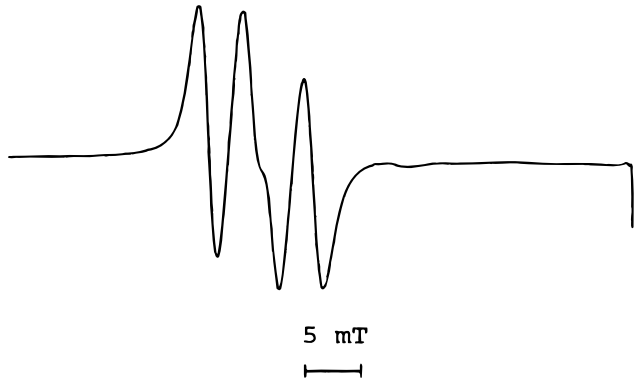

Figure 8. EPR spectrum for $[H_3Ru_3(\mu_3-COMe)(CO)_6(PPh_3)_3]^{1+}$ in dichloromethane at 20 °C.

time. The stability at room temperature follows the order NMeBz (hours) > OMe > SEt > Ph (seconds). The stability appears to be related to the oxidation potential, the lower the oxidation potential, the more stable the radical cation.

The EPR spectra of $[H_3Ru_3(\mu_3-CPh)(CO)_6(PPh_3)_3]^{1+}$, $[H_3Ru_3(\mu_3-CNMeBz)(CO)_6(PPh_3)_3]^{1+}$, and $[H_3Ru_3(\mu_3-COMe)(CO)_7(PPh_3)_2]^{1+}$ each show that the unpaired electron is coupled equivalently to each of the phosphorus atoms in the cluster. This suggests that no significant changes in the cluster geometry have occurred upon oxidation. In contrast, the EPR spectra of $[H_3Ru_3(\mu_3-CX)(CO)_6(PPh_3)_3]^{1+}$ (X = OMe or SEt) each show that the unpaired electron is coupled inequivalently to only two of the three phosphorus atoms in the molecule. EPR signals for $[H_3Ru_3(\mu_3-COMe)(CO)_6\{P(OMe)_3\}(PPh_3)_2]^{1+}$ and $[H_3Ru_3(\mu_3-COMe)(CO)_6(CNBz)(PPh_3)_2]^{1+}$ appear as triplets, most likely because of coincidentally equal hyperfine coupling constants to the nonequivalent axial PPh_3 ligands; there is no evidence for the presence of two isomers in either spectrum, and the center line of the triplet for $[H_3Ru_3(\mu_3-COMe)(CO)_6\{P(OMe)_3\}(PPh_3)_2]^{1+}$ is only slightly broader than that for $[H_3Ru_3(\mu_3-COMe)(CO)_6(CNBz)(PPh_3)_2]^{1+}$. These results can be explained in terms of a ligand isomerization from an axial site to an equatorial site following oxidation, reducing the symmetry of the cluster from C_{3v} to C_1, with large hyperfine couplings for trans phosphines and unobservable couplings for phosphines cis to the Ru−C bonds (Scheme 1).

The lack of resolvable hyperfine coupling for the equatorial phosphine ligands is confirmed by the EPR spectra of the oxidation products from treatment of $H_3Ru_3(\mu_3-COMe)(CO)_6\{\mu-dppm\}(PPh_3)$ (dppm = $(PPh_2)_2CH_2$) with ferricenium. The dppm ligand bridges equatorial sites on two different Ru atoms, whereas the PPh_3 ligand is axially coordinated. The EPR spectrum for the species proposed to be $[H_3Ru_3(\mu_3-COMe)(CO)_6\{\mu-dppm\}(PPh_3)]^{1+}$ is a doublet (a(^{31}P) 32 mT); no hyperfine coupling to the equatorial ^{31}P nuclei is observed.[32]

Another result which is consistent with axial to equatorial ligand isomerization as the explanation for the low symmetry of some of the 47-electron clusters comes from the oxidation of $H_3Ru_3(COMe)(CO)_6[(ax\text{-}PPh_2CH_2)_3CCH_3]$.[10b] This cluster should have a similar oxidation potential to that of $H_3Ru_3(COMe)(CO)_6(PPh_3)_3$, with the exception that ligand isomerization is not possible. Oxidation with Ag^+ in this case was shown to produce a very unstable radical cation, which displays a quartet EPR signal. Thus, ligand isomerization from an axial to equatorial site is the most likely explanation for the low symmetry of the radical cations $[H_3Ru_3(COMe)(CO)_6(PPh_3)_3]^+$ and $[H_3Ru_3(CSEt)(CO)_6(PPh_3)_3]^+$.

Radical Cation Structure and Isomerization. The spectroscopic data indicate that the structures of radical cations $[H_3Ru_3(CX)(CO)_6(PPh_3)_3]^{1+}$ (X = OMe, SEt) differ from those of the 48-electron precursors, whereas $[H_3Ru_3(CX)(CO)_6(PPh_3)_3]^{1+}$ (X = NMeBz, Ph) retain the all-axially substituted structure. The all-axial substitution adopted by $H_3Ru_3(CX)(CO)_6(PPh_3)_3$ is apparently due to steric factors. Smaller ligands such as pyridine, acetonitrile, and isocyanides preferentially occupy equatorial positions, and in fact, the kinetic product $H_3Ru_3(COMe)(CO)_6(ax\text{-}PPh_3)_2(ax\text{-}CNBz)$ was shown to rearrange to the more stable $H_3Ru_3(COMe)(CO)_6(ax\text{-}PPh_3)_2(eq\text{-}CNBz)$ within several hours ($k = 8.8 \times 10^{-5}$ s^{-1} at 19 °C). The isomerization of the radical cations indicates that the electronic preference for equatorial substitution is of greater importance relative to the steric preference for axial substitution. The all-axial structure is retained by $[H_3Ru_3(CX)(CO)_6(PPh_3)_3]^{1+}$ for the larger methylidyne substituents X = NMeBz and Ph. The rate of the isomerization is 4−5 orders of magnitude faster for the 47-electron species than for the 48-electron cluster. The rate constant for isomerization of $[H_3Ru_3(COMe)(CO)_6(ax\text{-}PPh_3)_3]^{1+}$ to the more stable $[H_3Ru_3(COMe)(CO)_6(ax\text{-}PPh_3)_2(eq\text{-}PPh_3)]^{1+}$ is 6.5 s^{-1} at 19 °C.

Rapid isomerizations for 17-electron complexes are well-known, but rarely can quantitative comparisons of 18- and 17-electron species be determined. Very recently, the relative rates for interconversion of isomers of $Cp^*IrCp_2Co_2(CO)_3$, involving bridging and terminal CO ligands, were determined to be 48-electron (1) ≪ 49-electron (10^4) ≪ 47-electron (10^8) species.[33]

Decomposition of the Radical Cations. Slow decomposition of $[H_3Ru_3(COMe)(CO)_6(PPh_3)_3]^{1+}$ occurs in solution under nitrogen. Overnight, the green solution gradually turns red in color. The major cluster products are starting material and a diamagnetic material which we propose to be $[H_3Ru_3(CO)_7(PPh_3)_3]^{1+}$, a

Table 5. EPR Spectral Data from Dichloromethane Solution

cluster	*T* (K)	*g*	$a(^{31}P)$, mT
$[H_3Ru_3(COMe)(CO)_6(PPh_3)_3]^+$	295	2.08 (dd)	4.0, 6.0
$[H_3Ru_3(CSEt)(CO)_6(PPh_3)_3]^+$	295	2.06 (dd)	3.5, 4.8
$[H_3Ru_3(CNMeBz)(CO)_6(PPh_3)_3]^+$	295	2.06 (q)	3.6
$[H_3Ru_3(CPh)(CO)_6(PPh_3)_3]^+$	225	2.09 (q)	2.6
$[H_3Ru_3(COMe)(CO)_6(P(OMe)_3)(PPh_3)_2]^+$	295	2.09 (t)	4.8
$[H_3Ru_3(COMe)(CO)_6(CNBz)(PPh_3)_2]^+$	295	2.09 (t)	4.9
$[H_3Ru_3(COMe)(CO)_7(PPh_3)_2]^+$	295	2.08 (t)	5.1
$[H_3Os_3(COMe)(CO)_7(PPh_3)_2]^+$	295	2.19 (br)	

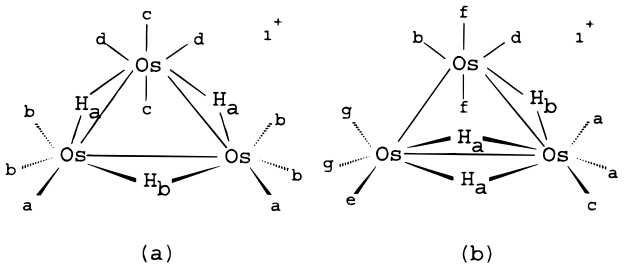

Figure 9. Possible structures for $[H_3Os_3(CO)_{10}]^{1+}$; structure b is the proposed structure.

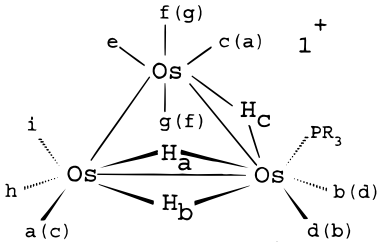

Figure 10. Proposed structure for $[H_3Os_3(CO)_9(PPh_3)]^{1+}$.

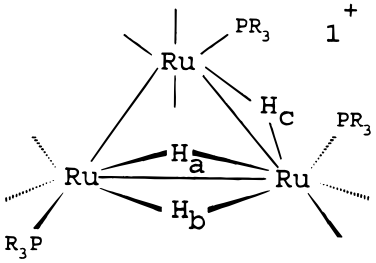

Figure 11. Proposed structure for $[H_3Ru_3(CO)_7(PPh_3)_3]^{1+}$.

new 46-electron cluster. Although no Ru clusters of this or related compositions had been previously reported, the Os analogues $[H_3Os_3(CO)_{10-n}L_n]^{1+}$ (L = PPh_3; n = 0, 1) have been prepared by protonation of unsaturated $H_2Os_3(CO)_{10-n}L_n$.[19] This formulation is based upon the ^1H and ^{31}P NMR data and comparison to the analogous cation $[H_3Os_3(CO)_9(PR_3)]^{1+}$. Decompositions of $[H_3Ru_3(CSEt)(CO)_6(PPh_3)_3]^{1+}$ and $[H_3Ru_3(COMe)(CO)_6(AsPh_3)_3]^{1+}$ form analogous products with similar hydride NMR resonances. The chemistries of $[H_3Ru_3(CSEt)(CO)_6(PPh_3)_3]^{1+}$ and its decomposition product are under investigation and will be the subject of a later paper. The NMR data are in Table 1. On the basis of the spectroscopic characterization of $[H_3Os_3(CO)_9(PPh_3)]^{1+}$ (vide infra), the proposed structure of $[H_3Ru_3(CO)_7L_3]^{1+}$ (L = PPh_3, $AsPh_3$) is shown in Figure 11. Attempts to purify these clusters, or their deprotonated forms, proved unsuccessful, due to their instability.

The likely mechanism by which the radical cations decompose is attack by PPh_3, released by decomposition, at the methyl group (eqs 3 and 4). The ^1H NMR spectra

$$[H_3Ru_3(COMe)(CO)_6(PPh_3)_3]^{1+} + PPh_3 \rightarrow H_3Ru_3(CO)_7(PPh_3)_3 + MePPh_3^{1+} \quad (3)$$

$$H_3Ru_3(CO)_7(PPh_3)_3 + [H_3Ru_3(COMe)(CO)_6(PPh_3)_3]^{1+} \rightarrow [H_3Ru_3(CO)_7(PPh_3)_3]^{1+} + H_3Ru_3(COMe)(CO)_6(PPh_3)_3 \quad (4)$$

of product solutions from decomposition of $[H_3Ru_3(COMe)(CO)_6(PPh_3)_3]^{1+}$ contain a doublet at 2.80 ppm (J 13 Hz), attributed to $[MePPh_3]^{1+}$ in a 1:1 molar ratio to $[H_3Ru_3(CO)_7(PPh_3)_3]^{1+}$ and substantial amounts of $H_3Ru_3(COMe)(CO)_6(PPh_3)_3$ are also present when the decomposition proceeds in the absence of added CO.

No cluster products were identified from the decomposition of the trisubstituted NMeBz or Ph analogues. However, for $H_3Ru_3(COMe)(CO)_8(PPh_3)$ and $H_3Ru_3(COMe)(CO)_7(PPh_3)_2$, decomposition regenerates starting material with low recovery. We were unable to isolate pure materials due to decomposition during purification by TLC or recrystallization.

Oxidations of the osmium alkylidyne clusters $H_3Os_3(COMe)(CO)_{9-n}(PPh_3)_n$ (n = 0−2) were examined to confirm the nature of the decomposition reaction of the radical cations $[H_3Ru_3(COMe)(CO)_6L_3]^{1+}$. The Os clusters show similar electrochemical behavior to their Ru analogues (Table 3), with the parent carbonyl and monosubstituted clusters showing an irreversible oxidation wave and the disubstituted cluster displays a quasi-reversible wave followed by an irreversible wave. Oxidation of $H_3Os_3(COMe)(CO)_7(PPh_3)_2$ with Ag^+ produces a green solution, which displays a singlet EPR signal (Table 5). No hyperfine coupling to phosphorus is observed, but the line width of the signal is quite broad. Addition of 1 equiv of Ag^+ to a dichloromethane solution of $H_3Os_3(COMe)(CO)_8(PPh_3)$ caused the yellow solution to turn fleetingly green before turning yellow again. ^1H NMR analysis of this solution indicated the presence of $[H_3Os_3(CO)_9(PPh_3)]^{1+}$, as well as starting material and other unidentified products. Treatment of the solution with methanol allowed for the recovery of $H_2Os_3(CO)_9(PPh_3)$ in 34% yield after TLC. This indicates that the net loss of the methyl radical, leading to the formation of $[H_3M_3(CO)_{10-n}L_n]^{1+}$ (M = Ru, L = PPh_3, $AsPh_3$, n = 3; M = Os, L = PPh_3, n = 1), is indeed a pathway for radical cation decomposition.

These clusters are formally unsaturated, having 46-valence electrons, a factor which may account for their instability. Carbon monoxide reacts with $[H_3Ru_3(CO)_7(PPh_3)_3]^{1+}$ within minutes. The red product displays an IR spectrum identical to the product of CO with the 47-electron $[H_3Ru_3(COMe)(CO)_6(PPh_3)_3]^{1+}$, which is char-

acterized as $[HRu_3(CO)_9(PPh_3)_3]^{1+}$ (vide infra), a 48-electron cluster.

Protonation of $H_2Os_3(CO)_{10}$ and $H_2Os_3(CO)_9(PPh_3)$. Because we were unable to purify $[H_3Ru_3(CO)_7L_3]^{1+}$, we could obtain limited information concerning the structure. The alternative synthetic pathway available for the osmium analogues provided a means of obtaining complete spectroscopic characterization. We, therefore, reinvestigated the structures of $[H_3Os_3(CO)_9(PPh_3)]^{1+}$ and $[H_3Os_3(CO)_{10}]^{1+}$ by ^1H, ^{13}C, and ^{31}P NMR spectroscopy. Johnson, Lewis, and co-workers had originally proposed two possible structures for $[H_3Os_3(CO)_{10-n}L_n]^{1+}$ (Figure 9, structures a and b) which were consistent with the available ^1H NMR data (Experimental Section).[19] These workers preferred the structure shown in Figure 9 a. However, the ^{13}C NMR data (Experimental Section) which we obtained are consistent with the structure shown in Figure 9b, not Figure 9a. For structure a, no more than four carbonyl resonances are expected from the C_s symmetry. However, the observed ^{13}C NMR spectrum displays seven carbonyl resonances, as expected for the C_1 symmetry of structure b. Tentative assignments of the NMR resonances in the Experimental Section are according to Figure 9b.

Further evidence for this structure is obtained from the spectra of $[H_3Os_3(CO)_9(PPh_3)]^{1+}$. The structure of $H_2Os_3(CO)_9(PPh_3)$ has C_s symmetry, with the phosphine ligand occupying an equatorial site on a hydride-bridged metal atom; the ^{13}C NMR spectrum contains the expected 2:2:2:1:1:1 pattern.[34] Protonation of this cluster to form the analogue to Figure 9, structure a or b, would not change the symmetry, and a similar pattern would be expected. However, the low symmetry evident in the ^{13}C NMR spectra is indicative of the structure in Figure 10. This structure is identical to the one adopted by the isoelectronic cluster $H_3Os_3(CO)_9(SiPh_3)$, for which the structure has been determined crystallographically.[35] The carbonyl assignments in the Experimental Section and Figure 10 are made using both the coupled and decoupled spectra, assuming that trans couplings to both phosphorus and hydrogen are large and cis couplings are small. The ^1H NMR spectrum of $[H_3Os_3(CO)_9(PPh_3)]^{1+}$ displays three hydride resonances, two of which have phosphorus coupling constants characteristic of a cis P−H relationship (7.3 and 9.3 Hz) and the third which has an unusually large coupling constant (30.5 Hz), indicative of a trans phosphorus−hydride relationship required by the structure in Figure 10.

Chemical Reactivity of the Radical Cation Cluster $[H_3Ru_3(COMe)(CO)_6(PPh_3)_3]^+$. An examination of the reactivities for the radical cluster $[H_3Ru_3(COMe)(CO)_6(PPh_3)_3]^+$ with various reagents on the electrochemical time scale did not afford much information. The cyclic voltammogram of $H_3Ru_3(COMe)(CO)_6(PPh_3)_3$ in dichloromethane at 100 mV/s was unaffected by the addition of 1−10 equiv of methyl iodide, benzyl bromide, acetonitrile, alkynes, or pyridine to the electrochemical cell. This suggested that the radical cation cluster was too stable to undergo ligand substitution, atom transfer, or other reactions on the time scale of the cyclic voltammetric experiment.

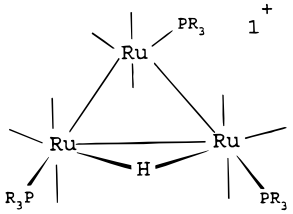

Figure 12. Proposed structure for $[HRu_3(CO)_9(PPh_3)_3]^{1+}$.

Since $[H_3Ru_3(COMe)(CO)_6(PPh_3)_3]^{1+}$ has a reasonable lifetime, we were able to examine its reactions with various reagents. Addition of chloride, acetonitrile, or pyridine to solutions of the 47-electron species, generated by oxidation with ferricenium, caused regeneration of the 48-electron precursor in yields of up to 60%. Disproportionation induced by donor ligands is a common reaction of 17-electron species. Slow decomposition in the absence of added Lewis bases gives the 46-electron species $[H_3Ru_3(CO)_7(PPh_3)_3]^{1+}$, in addition to $MePPh_3^{1+}$ and varying amounts of $H_3Ru_3(COMe)(CO)_6(PPh_3)_3$. Addition of CO at 1 atm causes rapid (<15 min) decomposition to $[HRu_3(CO)_9(PPh_3)_3]^{1+}$, and varying amounts of $H_3Ru_3(COMe)(CO)_7(PPh_3)_2$, $H_3Ru_3(COMe)(CO)_8(PPh_3)$, and $MePPh_3^{1+}$, were identified in the ^1H NMR spectrum of the product mixture. After workup, red-brown crystals of $[HRu_3(CO)_9(PPh_3)_3][BPh_4]$ were isolated in 30% yield (based upon the initial amount of $H_3Ru_3(COMe)(CO)_6(PPh_3)_3$), along with 23% recovery of the latter. The disappearance of the radical cation under CO is faster than its decomposition in the absence of CO or in the presence of 1 equiv of PPh_3. Characterization of the product $[HRu_3(CO)_9(PPh_3)_3][BPh_4]$ is based upon its IR spectrum, ^1H and ^{31}P NMR spectra, mass spectrum, and elemental analysis. The mass spectrum displays a low intensity ion at *m/e* 1344, with a higher intensity ion at *m/e* 1316; computer fitting of the mass envelope of the latter is consistent with the composition $[HRu_3(CO)_8(PPh_3)_3]^{1+}$ and suggests $[HRu_3(CO)_9(PPh_3)_3]^{1+}$ as the composition of the molecular ion. A structure which is consistent with the spectroscopic data is shown in Figure 12, analogous to structures of previously characterized $[HOs_3(CO)_9(PR_3)_3]^{1+}$, which can be prepared by protonation of $Os_3(CO)_9(PR_3)_3$.[36] The solution displays three ^{31}P signals, with one large $^{31}P-^{31}P$ coupling constant, which is consistent with the presence of two PPh_3 ligands trans to one another across a Ru−Ru bond. The ^1H NMR spectrum contains a single hydride resonance at −17.05 (dt, J_{PH} 3, 6 Hz) ppm, consistent with two PR_3 ligands cis to a bridging hydride and a third further removed; the ^1H NMR signal is similar to that reported for $[HOs_3(CO)_9(PR_3)_3]^{1+}$, e.g. PMe_2Ph −18.93 (t, J_{PH} 9.7 Hz).[36] The IR spectrum for $[HRu_3(CO)_9(PPh_3)_3]^{1+}$ (IR (CH_2Cl_2) 2096 vw, 2064 m,

(32) Bierdeman, D. J.; Kourouklis, D.; Keister, J. B. Unpublished results.

(33) Geiger, W. E.; Shaw, M. J.; Wünsch, M.; Barnes, C. E.; Foersterling, F. H. *J. Am. Chem. Soc.* **1997**, *119*, 2804.

(34) ^1H and ^{13}C NMR data for $H_2Os_3(CO)_9(PPh_3)$ in deuteriochloroform solution: ^{13}C NMR 176.8 (2 C, d, J_{CP} 13.5 Hz), 177.3 (1 C), 181.6 (2 C, d, J_{CP} 11.0 Hz), 183.2 (1 C), 184.1 (1 C), 185.4 (2 C) ppm; ^1H NMR −10.3 ppm (d, J_{PH} 7.2 Hz).

(35) Willis, A. C.; Einstein, F. W. B.; Ramadan, R. M.; Pomeroy, R. K. *Organometallics* **1983**, *2*, 935.

(36) (a) Bradford, C. W.; Nyholm, R. S. *J. Chem. Soc., Dalton Trans.* **1973**, 529. (b) Deeming, A. J.; Johnson, B. F. G.; Lewis, J. *J. Chem. Soc. A* **1970**, 2967. (c) Deeming, A. J.; Donovan-Mtunzi, S.; Kabir, S. E.; Hursthouse, M. B.; Abdul Malik, K. M.; Walker, N. P. C. *J. Chem. Soc., Dalton Trans.* **1987**, 1869.

2026 vs, 2011 sh, 1992 vw, 1967 w cm^{-1}) is almost identical with that reported for $[HOs_3(CO)_9(PPh_3)_3]Br$ (IR($CDCl_3$) 2097 w, 2064 m, 2021 vs, 2007 sh, 1985 w, 1965 w cm^{-1}).[36a] One caveat: we have been unable to prepare the equivalent material by protonation of $Ru_3(CO)_9(PPh_3)_3$ with CF_3CO_2H, CH_3SO_3H, or CF_3SO_3H in dichloromethane or chloroform solution, rather decomposition to a yellow solution, containing no hydride resonance, occurs upon mixing. Dissolution in sulfuric acid, followed by addition of aqueous ammonium hexfluorophosphate, produced a very small amount of a red solid having an IR spectrum similar to that attributed to $[HRu_3(CO)_9(PPh_3)_3]^{1+}$, but the amount was too small to allow purification and complete characterization.

Conclusion

The radical cations $[H_3Ru_3(CX)(CO)_6(PPh_3)_3]^{1+}$ have been prepared by chemical or electrochemical oxidations of the appropriate 48-electron, neutral precursor. These 47-electron clusters are surprisingly unreactive. Monometallic 17-electron complexes undergo extremely rapid halogen-atom abstraction and associative ligand substitutions.[1] These clusters do not react with the halogen-atom donors chloroform and carbon tetrachloride. Hard donors such as chloride ion, pyridine, and acetonitrile induce disproportionation, regenerating the 48-electron starting material in fair yield. Reactions with triphenylphosphine occur by attack at the methyl group for X = OMe rather than at the metal centers. These 47-electron alkylidyne clusters are also less reactive than other 47-electron clusters in which the unpaired electron is in a metal−metal bonding orbital, such as $HRu_3(\mu_3\text{-}\eta^3\text{-}XCCRCR')(CO)_{9-n}L_n$[37] or $H_2Ru_3(\mu_3\text{-}\eta^2\text{-}XCCR)(CO)_{9-n}L_n$.[23] The possible explanations for the low reactivity are that (1) the unpaired electron is delocalized over the entire $Ru_3(CX)$ framework, stabilizing the radical, cf. a 17-electron monometallic complex, (2) the unpaired electron is in a bonding orbital which is inaccessible to external reagents, and (3) the Ru−C bond strength is significantly greater than the Ru−Ru bond strength, stabilizing the radical, cf. 47-electron clusters in which the SOMO has metal−metal bond character.

Acknowledgment. This work was funded by a grant from the National Science Foundation (Grant No. CHE9213695) to J.B.K.

Supporting Information Available: Text giving the syntheses of $H_3Ru_3(COMe)(CO)_{9-n}(PPh_3)_n$ ($n = 1-3$) and $H_3Ru_3(CPh)(CO)_6(PPh_3)_3$ and tables of ^1H and ^{31}P NMR data (Table 1S), IR data (Table 2S), and data used for ligand additivity fitting (Table 3S) (5 pages). Ordering information is given on any current masthead page.

OM970769T

(37) Yao, H.; McCargar, R. D.; Allendoerfer, R. D.; Keister, J. B. *Organometallics* **1993**, *12*, 4283.